Journal of Catalysis 269 (2010) 255–268

Contents lists available at ScienceDirect

Journal of Catalysis

journal homepage: www.elsevier.com/locate/jcat

Activity, selectivity, and adsorbed reaction intermediates/reaction side products in the selective methanation of CO in reformate gases on supported Ru catalysts

S. Eckle, Y. Denkwitz, R.J. Behm *

Institute of Surface Chemistry and Catalysis, Ulm University, D-89069 Ulm, Germany

ARTICLE INFO

Article history:
Received 19 July 2009
Revised 29 October 2009
Accepted 30 October 2009
Available online 29 December 2009

Keywords:
Selective CO methanation
CO removal
Supported Ru catalyst
Selectivity
Activity
Mechanism

ABSTRACT

The reaction behavior and mechanistic aspects of the selective methanation of CO over two supported Ru catalysts, a Ru/zeolite catalyst and a Ru/Al_2O_3 catalyst, in CO_2 containing reaction gas mixtures were investigated by temperature-screening measurements, kinetic measurements and in situ diffuse reflectance infrared Fourier transform spectroscopy (DRIFTS) measurements. The influence of other components present in realistic reformate gases, such as H_2O and high amounts of CO_2, on the reaction behavior was evaluated via measurements in increasingly realistic gas mixtures. Temperature screening and kinetic measurements revealed a high activity of both catalysts, with the Ru mass-normalized activity of the Ru/zeolite catalyst exceeding that of the Ru/Al_2O_3 catalyst by about one order of magnitude. Approaching more realistic conditions, the conversion–temperature curve was shifted slightly upwards for the Ru/Al_2O_3 catalyst, whereas for the Ru/zeolite catalyst it remained unaffected. The selectivity was highest for the Ru/zeolite catalyst, where in parallel to full conversion of CO the conversion of CO_2 remained below 10% over a 40 °C temperature window. During selective methanation on the Ru/Al_2O_3 catalyst, CO_2 was converted even though CO was not completely removed from the feed. Transient DRIFTS measurements, following the build-up and decomposition of adsorbed surface species in different reaction atmospheres and in the corresponding CO-free gas mixtures, respectively, provide information on the formation and removal/stability of the respective adsorbed species and, by comparison with the kinetic data, on their role in the reaction mechanism. Consequences on the mechanism and physical reasons underlying the observed selectivity are discussed.

1. Introduction

Economically and ecologically efficient techniques for the production of sufficiently pure H_2 are a prerequisite for the introduction of H_2 based energy technologies [1]. Today, H_2 is mainly produced by steam reforming/partial oxidation of fossil fuels [2–7], which, among other components, leaves CO (1–8%) and substantial amounts of CO_2 (up to 20%) in the resulting H_2-rich gas mixture ('reformate'). For the operation of low-temperature polymer electrolyte fuel cells (PEFCs), the resulting H_2-rich gas should be free of catalyst poisons, in particular the CO content has to be reduced to $\leqslant$10 ppm under steady-state conditions [8] (<1 ppm after 2015 [9]) [10], which is most commonly achieved catalytically, by a combination of the water gas shift (WGS) reaction and the preferential oxidation of CO (PROX) [2,3,6,11,12]. In cost sensitive, small scale applications, however, methanation of the CO may be a more attractive process for CO removal compared to the PROX reaction, since it uses the H_2 present in the feed gas and avoids the need for an additional unit for O_2 dosing [4]. The losses of H_2 are tolerable, as long as the initial CO contents, after the WGS reaction, are low (0.5%). Precondition for this concept, however, is that the reaction is highly selective for the methanation of CO and that CO_2 methanation is essentially inhibited, otherwise the losses of hydrogen would become intolerable [4,13]. This is the background of the present study, where we investigated (i) the performance of two commercial-supported Ru catalysts, a zeolite-supported catalyst developed for these purposes and, for comparison, a standard Ru/Al_2O_3 catalyst, in the selective methanation of CO and (ii) mechanistic details of the reaction, aiming at a physical understanding of the reaction and the resulting high selectivities.

The CO methanation reaction is closely related to the Fischer–Tropsch reaction, where higher hydrocarbons are produced by the reaction of CO and H_2 [14,15], and accordingly, the most active catalysts in the Fischer–Tropsch reaction, oxide supported Fe, Co, Ni, and Ru catalysts [14,15], were identified also as the most active catalysts for the CO methanation reaction [16–22]. Also the methanation of CO_2 over Ru catalysts was investigated in a number of studies, e.g., in [23,24]. Catalysts with Ru as active component showed a high selectivity towards CO methanation in CO_2 containing gas mixtures [17,21,22,25–27]. Several authors [28–30]

* Corresponding author. Fax: +49 731 50 25452.
E-mail address: juergen.behm@uni-ulm.de (R.J. Behm).

0021-9517/$ - see front matter © 2009 Elsevier Inc. All rights reserved.
doi:10.1016/j.jcat.2009.10.025

proposed that the use of zeolites as support for Ru catalysts results in a higher selectivity for the selective methanation of CO compared to Ru/Al_2O_3 or Ru/SiO_2 catalysts, which they explained by a stronger metal-support interaction. Furthermore, because of their large surface areas, zeolites are likely to favor the formation of small Ru particles and to stabilize these against sintering; and, their well-defined pore structure may result in a narrower particle size distribution [31]. The resulting small Ru particle size was suggested to have a positive effect on the catalyst's activity [27,32,33]. Other groups, however, assumed that small particles and a high dispersion are counterproductive for the activity [21,34,35]. The surface species formed during reaction were characterized by in situ infrared spectroscopy studies on different Ru-catalysts. Different types of adsorbed CO adsorbed on the Ru particles, e.g., CO_{ad} on oxidized Ru, linear and bridged CO_{ad} on Ru^0, surface formates and/or surface carbonates as well as adsorbed $CH_{x,ad}$ species were observed during CO methanation on the catalysts [25,36–41]. From these studies it was not clear, however, whether there is a preference for a specific type of CO_{ad} as active species, and if so, for which of them. Formates and carbonates are commonly interpreted as side products.

CH_x species had been proposed by Ekerdt and Bell [37] and later by Yamasaki et al. [38] as reaction intermediates. The latter authors showed in a very detailed in situ IR study that upon changing from a $^{12}CO/H_2$ reaction atmosphere to a $^{13}CO/H_2$ gas mixture the signals related to $^{12}CH_{x,ad}$ species disappeared, while signals related to the corresponding $^{13}CH_{x,ad}$ species were growing in [38]. They also estimated concentrations of CH_2 and CH_3 groups present on the surface under steady-state conditions. Assuming that these groups belonged to adsorbed C_xH_y hydrocarbon chains, they could calculate the average length of the C_xH_y hydrocarbon chains. Based on these data they proposed a complex mechanism for the CO methanation reaction, where $CH_{x,ad}$ species act as reaction intermediates and CH_4 formation proceeds via formation and decomposition of adsorbed hydrocarbon chains [38]. However, since in the SSITKA-type (steady-state isotope transient kinetic analysis) experiments the $CH_{x,ad}$ removal rate in H_2 was not quantified and compared to the CH_4 formation rate, it is not clear, whether the reactive removal of the $CH_{x,ad}$ species observed in IR is really the rate-limiting step in the dominant reaction pathway, which would mean that these species represent reaction intermediates in that pathway, or whether they should better be considered as spectator species or as reaction intermediates in a minority pathway (side reaction). Further information on mechanistic aspects can be derived from recent density functional theory (DFT) studies [42–46].

In the present paper, we investigated the CO methanation reaction in a number of different reaction atmospheres, going from pure H_2/CO and H_2/CO_2 mixtures to more realistic reaction mixtures, over a Ru/zeolite and a Ru/Al_2O_3 catalyst. In the first part, we characterized the activity, selectivity and stability of the two catalysts in conversion measurements and in kinetic measurements under differential reaction conditions, determining reaction rates, activation energies and reaction orders. In the second part, the formation and their accumulation with time of different surface species under reaction conditions as well as their decomposition in CO-free atmosphere (H_2/N_2 mixtures) was followed in transient in situ diffuse reflection IR Fourier transform spectroscopy (DRIFTS) measurements, performed under comparable reaction conditions (differential conversion, identical gas mixtures and reaction temperatures) as used in the kinetic measurements and compared to reaction and mass spectrometric transient data. The correlation between the activity and the build-up of surface species during the reaction under different reaction conditions and between the removal of adsorbates and CH_4 formation in transients in CO-free atmosphere on both Ru catalysts as well as consequences for the reaction pathway are discussed.

2. Experimental

2.1. Catalyst properties

Two Ru catalysts were investigated, a Ru/zeolite catalyst prepared by Süd-Chemie AG with 2.2 wt.% Ru loading and a commercial 5.0 wt.% Ru/Al_2O_3 catalyst (Johnson Matthey). The BET surface areas were determined by N_2 adsorption to 100 and 410 $m^2\,g^{-1}$ for the Ru/Al_2O_3 and the Ru/Zeolite catalyst, respectively. The Ru oxidation state was determined by X-ray photoelectron spectroscopy (XPS; PHI 5800 ESCA system), using monochromatized Al Kα radiation. For the as-received catalysts, without additional pre-treatment, most of the surface Ru is present as Ru oxide, with a Ru^{4+}/Ru^0 ratio of 2:1. This is true for both catalysts. Similar results were obtained also after reactive pre-treatment (description see Section 2.2). Most likely, any changes induced by the reactive pre-treatment are counteracted by the transport through air from the reactor used for pre-treatment to the XPS spectrometer. The Ru particle size was investigated by different methods. For the Ru/zeolite catalyst, X-ray diffraction (XRD) showed reflections related to RuO_2 before reactive conditioning (used as received, conditioning see Section 2.2), corresponding to RuO_2 domain/nanoparticle sizes of 10 nm diameter (Debye–Scherrer). After reactive conditioning for 100 min., the RuO_2-related XRD reflection decreased significantly in intensity. On the other hand, except for a small shoulder at a support-related reflection, no signal related to metallic Ru was observed, indicative of very small (<1 nm diameter) Ru nanoparticles or grains. On a used catalyst, after 1800 h on stream, the diffractogram reveals metallic Ru nanoparticles or nanograins of 2 nm mean diameter.

For the Ru/Al_2O_3 catalyst, the Ru particle size was determined by TEM imaging to 2–3 nm diameter. On the Ru/zeolite catalyst, in contrast, high resolution TEM imaging was complicated by electron beam-induced decomposition of the zeolite. The images showed a very inhomogeneous distribution of Ru particles, with few individual particles (10–20 nm diameter) and agglomerates of Ru particles, in addition to larger areas without visible nanoparticles (representative TEM images are given as Supplementary material, Fig. 1S).

H_2 adsorption experiments performed on the two catalysts after reduction in H_2 (30 min, 200 °C) yielded active surface areas of 3.7 $m^2\,g^{-1}$ (Ru/Al_2O_3) and 0.095 $m^2\,g^{-1}$ (Ru/zeolite), which would correspond to dispersions/Ru particles sizes of 15%/6.5 nm and <1%/113 nm, respectively. (It should be noted that higher reduction temperatures up to 300 °C had no effect on the active surface area, above that temperature the active surface area decreases, probably due to agglomeration.) Additional adsorption experiments performed on a temporal analysis of products (TAP) reactor at −30 °C after reactive conditioning (100 min, see Section 2.2) yielded active surface areas of 2.8 $m^2\,g^{-1}$ and 0.7 $m^2\,g^{-1}$ for the Ru/Al_2O_3 and the Ru/zeolite catalyst, respectively, which would correspond to dispersions/particle sizes of 12.5%/8 nm (Ru/Al_2O_3) and 6.3%/15 nm (Ru/zeolite). After 1000 min reaction, the respective values were 2.35 $m^2\,g^{-1}$/10.5%/10 nm (Ru/Al_2O_3) and 0.7 $m^2\,g^{-1}$/6.5%/15 nm (Ru/zeolite). Obviously, the dispersions and particle sizes derived from the adsorption experiments are incompatible with those determined by TEM or XRD. We explain this discrepancy by assuming that also after conditioning a significant fraction of the Ru nanoparticle surface is still oxidized and therefore does not adsorb hydrogen. During reaction, the oxidized Ru surface is further reduced in the reaction atmosphere, but at the same time, an increasing fraction of the active Ru surface area is

covered by the build-up of carbonaceous adsorbates (see Section 3.3.2). Hence, the size of the Ru nanoparticles in the zeolite is still unclear, and this is true also for the question of whether very small (TEM invisible) Ru particles are present in the sample, in addition to larger particles. On the other hand, the active (metallic) Ru surface area of the catalyst after conditioning and during reaction, as determined by hydrogen adsorption, is rather well defined and allows the determination of the intrinsic activity of the Ru surface via turn-over frequencies (see next section).

2.2. Temperature screening and kinetic measurements

The temperature screening, the kinetic, and the mass spectrometric transient measurements were carried out at atmospheric pressure in a quartz tube micro reactor. (The catalysts were used as received, but the measurement procedure largely resembles the pre-treatment procedure (Section 2.2) and essentially includes this in the initial heating up to 190 °C). In the temperature screening measurements and in the mass spectrometric transients (Fig. 7), we used 210 mg and 100 mg catalyst powder, respectively. For the kinetic measurements, 18.8 mg (Ru/zeolite) or 55 mg (Ru/Al_2O_3) catalyst powder, respectively, were used. These amounts of catalyst were sufficiently low to yield differential reaction conditions (conversion <15%). The Ru/zeolite catalyst was diluted with SiO_2 (total mass 210 mg) to obtain comparable catalyst volumes and hence space velocities. For Ru/Al_2O_3, no dilution was necessary. During the temperature screening measurements, the temperature was raised from 150 °C in increments of first 10 °C, then 5 °C (in the range of increasing conversion) and finally 20 °C, ending at 270 °C (in CO_2-free reaction mixtures) or 410 °C (in CO_2-containing reaction mixtures). Each temperature was measured for 2 h, where the conversion did not change any more and steady-state can be assumed. The experiments were carried out with a gas flow of 41.6 Nml min^{-1} in the different gas mixtures (for compositions, see Tables 1 and 2). To maintain identical space velocities in the temperature screening measurements (5000 h^{-1}), the gas flow was adjusted accordingly for the more voluminous Ru/Al_2O_3 catalyst in these measurements. In CO_2 containing gas mixtures, the selectivity for CO methanation was determined by dividing the CH_4 content calculated from the conversion of CO by the measured CH_4 content. The deactivation measurements were performed at 190 °C reaction temperature, following the reaction rate over 1000 min under differential reaction conditions. Prior to determining reaction orders and activation energies, the catalyst was exposed to the reaction atmosphere for 1000 min to assure stable catalyst and reaction conditions. The activity was monitored with decreasing partial pressure (temperature) and back to verify stable catalyst conditions during these measurements. The gas mixtures were prepared via mass flow controllers (Hastings HFC-202, and Bronkhorst F201C-FA-88 V). Defined amounts of water were added to the gas stream by passing it through a thermostated water bath. Incoming and effluent gases were analyzed by on-line gas chromatography with a CO detection limit of ca. 20 ppm (Chrompak 9001 GC), using H_2 as carrier gas. Mass spectrometric transients were measured by an ion–molecule reaction mass spectrometer (IMR-MS) (Atomika IMR-MS SP 89) [47], which allows for the detection of CO (mass 28) without interference with N_2. Absolute amounts of desorbing gases were determined via calibration of the IMR-MS. High-purity reaction gases (CO 4.7, H_2 5.0, N_2 6.0, CO_2 5.0, CH_4 4.5 from Westphalen) were used. The conversions were determined by the CO partial pressure. Evaluation of the Weisz criterion showed the absence of mass transport-related problems [48]. Prior to the experiments, the catalysts were heated up in a N_2 stream to 150 °C. Subsequently, the catalysts were heated to the reaction temperature in reaction gas (41.6 Nml min^{-1}).

2.3. Infrared measurements

In situ IR measurements were performed by DRIFTS, using a commercial in situ reaction cell (Harricks, HV-DR2) [49]. The spectra were recorded in a Magna 560 spectrometer (Nicolet), equipped with a MCT narrow-band detector. Gas mixtures were prepared as described above, and similar gas flows were used (41.6 Nml min^{-1}). Around 30 mg of diluted catalyst (1:5 with Al_2O_3) were used as catalyst bed. Typically, 400 scans were co-added for one spectrum. The intensities were evaluated in Kubelka–Munk units, which are linearly related to the adsorbate concentration [50] (for exceptions see [51]). Background subtraction and normalization of the spectra were performed by subtracting spectra recorded in a flow of N_2 at the reaction temperature directly after catalyst conditioning. To correct for changes in the reflectivity during reaction, the spectra were scaled to a constant background; for the evaluation of the peak intensities in Fig. 6, the spectra were normalized to similar intensities directly aside the peak.

Table 1
Reaction temperature for 50% and 100% CO/CO_2 conversion in the methanation reaction on 210 mg Ru/Al_2O_3 catalyst (5 wt.% Ru, GSVH: 5000 h^{-1}).

Reaction gas	Reaction gas composition	T_{50} = 50% conversion (CO) (°C)	T_{100} = 100% conversion (CO) (°C)	T_{50} = 50% conversion (CO_2) (°C)	T_{100} = 100% conversion (CO_2) (°C)
Idealized reformate	0.6 kPa CO, 2.8 kPa N_2, rest H_2	200	210	–	–
CH_4-rich idealized reformate	0.6 kPa CO, 2.8 kPa N_2, 4.5 kPa CH_4, rest H_2	200	230	–	–
H_2O-rich idealized reformate	0.6 kPa CO, 2.8 kPa N_2, 5 kPa H_2O, rest H_2	205	230	–	–
CO_2-rich idealized reformate	0.6 kPa CO, 2.8 kPa N_2, 1.2 kPa CO_2, rest H_2	205	230	225	270
CO-free idealized reformate	1.2 kPa CO_2, 2.8 kPa N_2, rest H_2	–	–	205	250

Table 2
Reaction temperature for 50% and 100% CO/CO_2 conversion in the methanation reaction on 210 mg Ru/zeolite catalyst (2.2 wt.% Ru, GSVH: 5000 h^{-1}).

Reaction gas	Reaction gas composition	T_{50} = 50% conversion (CO) (°C)	T_{100} = 100% conversion (CO) (°C)	T_{50} = 50% conversion (CO_2) (°C)	T_{100} = 100% conversion (CO_2) (°C)
Idealized reformate	0.6 kPa CO, 2.8 kPa N_2, rest H_2	190	200	–	–
CH_4-rich idealized reformate	0.6 kPa CO, 2.8 kPa N_2, 4.5 kPa CH_4, rest H_2	190	210	–	–
H_2O-rich idealized reformate	0.6 kPa CO, 2.8 kPa N_2, 5 kPa H_2O, rest H_2	190	210	–	–
CO_2-rich idealized reformate	0.6 kPa CO, 2.8 kPa N_2, 1.2 kPa CO_2, rest H_2	170	190	330	410
CO-free idealized reformate	1.2 kPa CO_2, 2.8 kPa N_2, rest H_2	–	–	330	410

3. Results and discussion

3.1. Temperature screening experiments

In the first step, we explored the activity of the two Ru catalysts for the conversion of CO and CO_2 to CH_4 and the influence of CH_4, H_2O and CO_2 on the CO methanation reaction in different gas mixtures under integral reaction conditions (see Tables 1 and 2). Fig. 1 shows the temperature dependent conversions of CO and CO_2 on the Ru/Al_2O_3 (left panels) and Ru/zeolite catalysts (right panels). The upper and lower panels depict the conversion during the methanation reaction in CO_2-free and CO_2-rich gas mixtures, respectively. In the different gas mixtures, the CO conversion on both catalysts shows a typical S-shaped curve, starting at 150 °C with a very low conversion (<5%).

For reaction in a CO/H_2 mixture (idealized reformate, 0.6 kPa CO, 2.6 kPa N_2, rest H_2), 50% CO conversion to CH_4 (T_{50}) are reached at 200 and 190 °C for the Ru/Al_2O_3 and Ru/zeolite catalysts, respectively, under present reaction conditions (Fig. 1, top panels). After reaching full conversion, a further increase of the temperature had no effect on the CH_4 production on either catalyst. Full CO conversion is reached at 10 °C lower temperature on the Ru/zeolite catalyst than on the Ru/Al_2O_3 catalyst. Since the Ru loading of the Ru/zeolite catalyst (2.2 wt.%) is less than half of that of the Ru/Al_2O_3 catalyst (5 wt.%), its Ru mass-normalized activity is higher than that of the latter catalyst. Similar trends are observed when adding H_2O (H_2O-rich idealized reformate) or CH_4 (CH_4-rich idealized reformate) to the gas-mixture, with the differences in activity becoming slightly higher (Fig. 1, top panels; Tables 1 and 2). For both the H_2O-rich and the CH_4-rich reformate, the temperature dependence does not change for the Ru/zeolite catalyst. The Ru/Al_2O_3 catalyst behaves similarly in the CH_4-rich reformate, while in H_2O-rich reformate the T_{50} temperature is shifted to slightly higher values, from 200 to 205 °C.

Next, we followed the CO_2 methanation reaction in a CO-free reaction gas mixture (CO_2/H_2 mixture). The general shape of the temperature dependent CO_2 methanation curve is comparable to that for CO methanation in idealized reformate (0.6 kPa CO; 2.6 kPa N_2; rest H_2) for the Ru/Al_2O_3 catalyst, except for a slight shift to higher temperatures (CO_2 conversion: T_{50} = 205 °C, CO conversion: T_{50} = 200 °C, see Table 1). In contrast, on the Ru/zeolite catalyst the increase of the CO_2 conversion with increasing temperature is significantly slower. The temperature for 50% conversion (T_{50}) is shifted to 330 °C (CO methanation: T_{50} = 190 °C, see Table 2), and full conversion is reached only at 410 °C (CO methanation: 200 °C, see Table 2).

Adding CO to the gas-mixture (CO_2-rich idealized reformate: 0.6 kPa CO, 2.8 kPa N_2, 1.2 kPa CO_2, rest H_2), the general shape of the conversion curve for CO and CO_2 methanation does not change, neither for the Ru/zeolite nor for the Ru/Al_2O_3 catalyst (Fig. 1, bottom panels; Tables 1 and 2). For the Ru/Al_2O_3 catalyst, however, the CO_2 conversion curve is shifted to higher temperatures, and seems to be suppressed by the presence of CO, at least over a temperature range of 20 °C. The temperature for 50% CO_2 conversion is shifted from 205 °C in a CO_2/H_2 mixture to 225 °C in the presence of CO, in CO_2-rich idealized reformate. Nevertheless, CO_2 conversion starts already well before all CO is converted to CH_4. At 100% CO conversion (230 °C), the selectivity is 48%. On the other hand, for the Ru/zeolite catalyst, the CO_2 methanation reaction is only little affected by the presence of CO. Furthermore, the CO methanation is accelerated by the presence of CO_2, and 50% CO conversion was reached at 170 °C in CO_2-rich idealized reformate rather than at 190 °C in idealized reformate. In the presence of CO_2, the reaction is 100% selective for CO methanation on the Ru/zeolite catalyst up to 190 °C. Only at 230 °C, the CO_2 conversion reaches 10%, i.e., there is a temperature window of 40 °C where the selectivity for CO methanation is >85%.

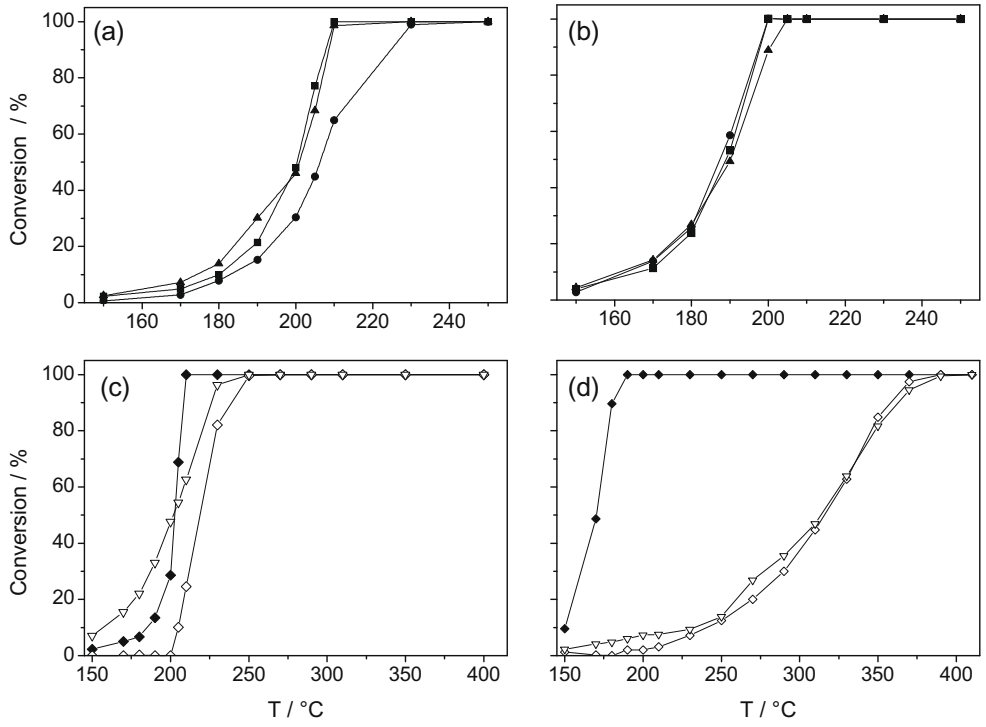

Fig. 1. Temperature dependence (150–400 °C) of the CO conversion (filled symbols) and CO_2 conversion (open symbols) on a Ru/Al_2O_3 (a, c) and a Ru/zeolite (b, d) catalyst (210 mg; GHSV: 5000 h^{-1}) in different reformate gases: ■: idealized reformate (0.6 kPa CO, 2.8 kPa N_2, rest H_2), ▲: H_2O-rich idealized reformate (0.6 kPa CO, 2.8 kPa N_2, 5 kPa H_2O, rest H_2), ●: CH_4-rich idealized reformate (0.6 kPa CO, 2.8 kPa N_2, 4.5 kPa CH_4, rest H_2); ♦, ◇: CO_2-rich idealized reformate (0.6 kPa CO, 2.8 kPa N_2, 1.2 kPa CO_2, rest H_2) and ▽: CO_2/H_2 mixture (1.2 kPa CO_2, 2.8 kPa N_2, rest H_2).

Comparison of the temperature screenings results with previously reported data is hardly possible, at least not on a quantitative scale, because of the different reaction conditions, reaction mixtures and procedures for catalyst pretreatment. For the Ru/zeolite catalyst, there are no previous studies on the CO methanation reaction at all. For CO methanation in idealized reformate on a Ru/Al_2O_3 catalyst, Randhava and Amirali [16] reported a T_{50} value (200 °C) which is similar to our result. It was measured, however, on a lower loaded 0.5 wt.% Ru/Al_2O_3 catalyst in 0.3% CO (rest H_2) at a significantly higher space velocity (GHSV: 36,000 h^{-1}, our measurement: GSHV: 5000 h^{-1}). They observed that the T_{50} value shifts to higher temperature with higher GHSV and attributed this to the lower contact time (CO conversion of 50% at 230 °C for a GHSV of 36,000 h^{-1}). Echigo and Tabata [13] performed temperature screening experiments on a 1 wt.% Ru/Al_2O_3 catalyst at a lower GHSV (7500 h^{-1}) in H_2O-rich reformate (0.54% CO, 20% H_2O, rest H_2) and in realistic reformate (0.54% CO, 21% CO_2, 20% H_2O, rest H_2). In the first gas mixture, they measured a T_{50} temperature of 190 °C, and full conversion (<10 ppm) was reached at 210 °C. Adding CO_2 to the gas mixture, the CO conversion at 190 °C dropped to about 45%, and full conversion was not reached up to 230 °C (maximum conversion 96% at 230 °C). Comparable to our observations for the Ru/Al_2O_3 catalyst, not all CO is converted, although the methane production exceeds the CO consumption. The CO_2 conversion starts already at 205 °C; at 230 °C the selectivity was 40%. Adding CH_4 to the gas-mixture did not change the performance of their catalyst. Dagle et al. [27] also investigated the methanation reaction in realistic reformate (0.9% CO, 24.5% CO_2, 5.7% H_2O, rest H_2) on differently loaded Ru/Al_2O_3 catalysts (3 wt.%, 5 wt.% and 7 wt.%, GHSV 13,500 h^{-1}). They observed the same T_{50} value (T_{50} = 205 °C) on their 5 wt.% Ru/Al_2O_3 catalyst as determined on our 5 wt.% Ru/Al_2O_3 catalyst, but at significantly higher CO, CO_2 and H_2O contents and at a higher space velocity. At higher temperatures, however, their catalyst became active for the reverse water gas shift (RWGS) reaction, which was evidenced by the onset of CO production at higher temperatures. Such effects were not observed in the present work, neither for the Ru/zeolite nor for the Ru/Al_2O_3 catalyst. The temperature for 99% conversion (100 ppm CO in the gas mixture) was lowest for the 5wt.% catalyst, and increased in the order 5 wt.% < 3 wt.% ≪ 7 wt.%.

In total, the activity, measured in terms of conversion curves and T_{50} values, and the selectivity of the Ru/Al_2O_3 catalyst in this work are comparable to those reported in previous studies [13,16,27]. The Ru/zeolite catalyst shows a comparable activity, despite of the much lower Ru content, and a significantly higher selectivity for the CO methanation in the presence of CO_2 over a wide temperature range.

3.2. Kinetic measurements

For more detailed information on the time-dependent activity and the stability of the catalysts under reaction conditions, we evaluated the reaction rates under differential reaction conditions (conversion < 15%) as a function of increasing time on stream, up to over 1000 min reaction time. This time was chosen since initial measurements showed only very slow changes in the reaction behavior after 800 min on stream. The activity is given in Ru mass normalized rates in Fig. 2. In addition, we used these data to calculate turn-over frequencies (TOFs) using the active Ru surface areas determined by H_2 adsorption in TAP reactor measurements (see previous section), which are listed in Table 3. As reaction temperature we used 190 °C. At this temperature, both Ru catalysts showed 100% selectivity in CO_2-rich idealized reformate in the temperature screening measurements (Fig. 1). The conversion was reduced by using smaller amounts of catalyst (see Section 2.2).

Fig. 2 illustrates the reactivity–time curves resulting for the two catalysts at 190 °C in different reaction atmospheres. In order to approach more realistic situations, we included two gas mixtures with higher CO_2 contents, namely semi-realistic reformate (0.6 kPa CO, 2.8 kPa N_2, 15.5 kPa CO_2, rest H_2) and H_2O-rich semi-realistic reformate (0.6 kPa CO, 2.8 kPa N_2, 15.5 kPa CO_2, 5 kPa H_2O, rest H_2), in addition to the idealized reformate and the CH_4-rich idealized reformate used also in the temperature screening experiments.

For reaction in idealized reformate (0.6 kPa CO, 2.8 kPa N_2, rest H_2; Fig. 2a), the catalysts exhibit initial reaction rates of 64×10^{-6} and 3.4×10^{-6} mol s^{-1} g_{Ru}^{-1} for the Ru/zeolite and the Ru/Al_2O_3 catalyst, respectively. At the beginning of the reaction, over ~50 min, the Ru/zeolite catalyst shows a slight increase in activity and then decays slowly, reaching ~80% of its maximum activity after 1000 min. In contrast, on the Ru/Al_2O_3 the reaction is about stable over the entire time on stream of 1000 min. The steady-state reaction rates for the Ru/zeolite and the Ru/Al_2O_3 catalyst are $64 \pm 1.5 \times 10^{-6}$ mol s^{-1} g_{Ru}^{-1} and $3.4 \pm 0.3 \times 10^{-6}$ mol s^{-1} g_{Ru}^{-1}, respectively, equivalent to TOFs of 135 and 4.4 s^{-1}. It should be noted that the TOF values are based on the active surface area determined by hydrogen adsorption measurements (TAP reactor measurements (Section 2.1)). Therefore deviations caused by missing very small Ru nanoparticles or clusters, e.g. in TEM images, do not affect these results. Changing to CH_4-rich idealized or semi-realistic reformate does not influence the activity and its characteristic development during 1000 min reaction for either of the two catalysts. In the semi-realistic gas mixture, both catalysts are 100% selective, which we associate with the high remaining CO partial pressure (10% CO conversion) and the low reaction temperature (CO_{ad} blocking of

Table 3
Reaction rates of the CO methanation reaction on different supported Ru catalysts and the respective reaction conditions (TOFs in this work are based on the active surface area determined by H_2 adsorption experiments).

Catalyst	Temperature (°C)	Reaction gas mixture	Rate × 10^6 (mol s^{-1} g_{cat}^{-1})	Rate × 10^6 (mol s^{-1} g_{Ru}^{-1})	TOF × 10^3 (s^{-1})	Reference
4.5 wt.% Ru/Al_2O_3	302	CO: H_2 (1:4)	0.16	3.56	–	[53]
0.5 wt.% Ru/Al_2O_3	250	1 kPa CO, 50 kPa H_2, rest He	0.536	107.2	15	[22]
0.5 wt.% Ru/Al_2O_3	250	1 kPa CO, 15 kPa CO_2, 50 kPa H_2, rest He	0.373	74.6	11	[22]
0.5 wt.% Ru/Al_2O_3	250	1 kPa CO, 15 kPa CO_2, 30 kPa H_2O, 50 kPa H_2, rest He	0.306	61.2	20	[22]
15 wt.% Ru/Al_2O_3	220	0.4 kPa CO, rest H_2	24.2	161	20	[21]
5 wt.% Ru/Al_2O_3	190	0.6 kPa CO, 2.8 kPa N_2, rest H_2	0.15 ± 0.027	3.43 ± 0.3	4.44	This work
5 wt.% Ru/Al_2O_3	190	0.6 k Pa CO, 15.5 kPa CO_2, 2.8 kPa N_2, 5 kPa H_2O rest H_2	0.19 ± 0.025	3.83 ± 0.5	4.96	This work
5 wt.% Ru/Al_2O_3	190	0.6 k Pa CO, 15.5 kPa CO_2, 2.8 kPa N_2, rest H_2	0.16 ± 0.023	3.14 ± 0.4	4.07	This work
5 wt.% Ru/Al_2O_3	190	0.6 k Pa CO, 4.5 kPa CH_4, 2.8 kPa N_2, 5 kPa H_2O rest H_2	0.22 ± 0.024	4.4 ± 0.4	5.7	This work
3 wt.% Ru/SiO_2	240	72 kPa H_2, 3.6 kPa CO, rest He	1.4	46.0	13	[52]
5 wt.% Ru/SiO_2	200	1 kPa CO, 90 kPa H_2	0.095	1.94	–	[54]
2.2 wt.% Ru/zeolite	190	0.6 k Pa CO, 2.8 kPa N_2, rest H_2	1.40 ± 0.035	63.9 ± 1.5	135	This work
2.2 wt.% Ru/zeolite	190	0.6 k Pa CO, 15.5 kPa CO_2, 2.8 kPa N_2, 5 kPa H_2O, rest H_2	0.7 ± 0.13	31.8 ± 4.7	67.2	This work
2.2 wt.% Ru/zeolite	190	0.6 k Pa CO, 15.5 kPa CO_2, 2.8 kPa N_2, rest H_2	1.33 ± 0.2	60.3 ± 4.7	127	This work
2.2 wt.% Ru/zeolite	190	0.6 k Pa CO, 4.5 kPa CH_4, 2.8 kPa N_2, rest H_2	1.42 ± 0.19	64.5 ± 8.3	136	This work

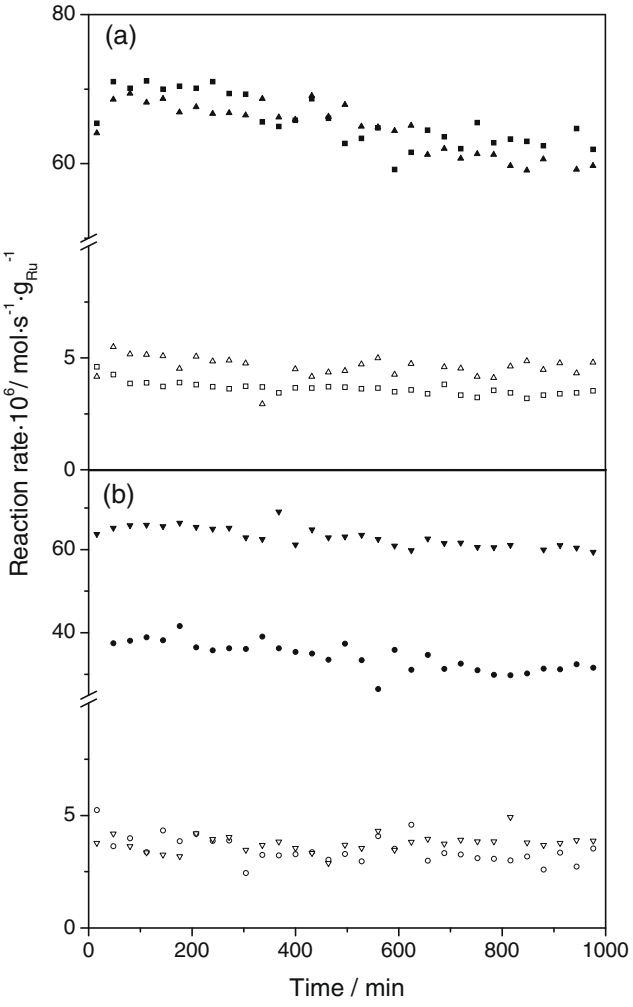

Fig. 2. Reaction rates on the Ru/zeolite (filled symbols, diluted 1:10 with SiO_2) and the Ru/Al_2O_3 (open symbols, diluted 1:3 with Al_2O_3) catalyst in different reformate gases: (a) ■, □: idealized reformate (0.6 kPa CO, 2.8 kPa N_2, rest H_2); (a) ▲, △: CH_4-rich idealized reformate (0.6 kPa CO, 2.8 kPa N_2, 4.5 kPa CH_4, rest H_2); (b) ▼, ▽: semi realistic reformate (0.6 kPa CO, 2.8 kPa N_2, 15.5 kPa CO_2, rest H_2); (b) ●, ○: H_2O-rich semi-realistic reformate (0.6 kPa CO, 2.8 kPa N_2, 15.5 kPa CO_2, 5 kPa H_2O, rest H_2).

the catalyst surface). In all the cases, the Ru/zeolite catalyst shows a significantly higher activity than the Ru/Al_2O_3 catalyst. It exceeds that of the latter catalyst by a factor of about 10 for the Ru mass-normalized reaction rate. The small differences between the rates measured for different gas compositions are within the precision of the measurements. A significantly lower activity (∼50%) is obtained, however, in H_2O-rich semi-realistic reformate, on the Ru/zeolite catalyst. The other characteristics, the low deactivation with time by about 20% over 1000 min and 100% selectivity remain unchanged. Long-term measurements over up to 1800 h, which will be the subject of a future paper, supported these trends. On the Ru/Al_2O_3 catalyst, the addition of water to semi-realistic reaction gases has essentially no consequences on the reaction behavior.

Comparing the Ru mass-normalized rates for the methanation reaction with results reported previously for reaction on supported Ru catalysts (see Table 3) [20–22,52–54], the Ru/zeolite catalyst exhibits a high activity at lower reaction temperature (190 °C) even in semi-realistic reformate. Only the Ru/Al_2O_3 catalyst studied by Kowalczyk et al. [21] shows a higher reaction rate, yet their measurement was performed at a higher temperature. The Ru/Al_2O_3 catalyst exhibits a lower activity compared to the rates reported for other Ru/Al_2O_3 catalysts (Table 3). However, one has to take into account that the reaction temperature and the gas compositions used in the previous studies differ considerably. Panagiotopoulou et al. [22] measured the CO methanation rate on a 0.5 wt.% Ru/Al_2O_3 catalyst at 250 °C in idealized reformate as well as in more realistic gas mixtures (see Table 3), and obtained higher reaction rates than determined in our work. The higher reaction temperature in their measurements has a positive effect on the activity, but they also used a gas mixture with higher CO and lower H_2 concentration, which has a negative influence on the activity [36]. Additionally, they used a different Ru loading, which may also affect the activity [27] (see Section 3.1).

Using turn-over frequencies as a measure of the intrinsic activity of the Ru particle surface rather than the Ru mass normalized rates for comparison (see Table 3), the very high activity of the Ru/zeolite catalyst is even more obvious, exceeding that of all other catalysts by a factor of at least 6.5, despite the lower reaction temperature in the present study (see Table 3). The general trends of the mass normalized activities, however, are reproduced. It is important to realize that the turnover frequencies reported in the different studies are based on different methods for determining the active Ru particle surface. Kowalczyk et al. [21] used O_2 chemisorption at 0 °C after reduction at 430 or 520 °C for 20 h. Subsequently, the catalyst was reduced at the same temperatures again and CO chemisorption was performed at room temperature (stoichiometries: 1.1 O atom per Ru surface atom, 0.6 CO molecule per Ru surface atom). Panagioptoulou et al. [22] performed H_2 chemisorption at 100 °C to calculate the Ru dispersion. All other groups [52,54,55] used reversible/irreversible H_2 chemisorption at room temperature to determine the Ru surface area and thus the Ru particle size. In the present study, we employed H_2 chemisorption at −30 °C (irreversible H_2 adsorption) to obtain almost full H_{ad} coverage (0.75 monolayer) on Ru, since hydrogen desorption starts at about this temperature only.

Comparing two 3 wt.% Ru/Al_2O_3 catalysts with 10 nm and 34 nm Ru particles, Dagle et al. [27] found 99% CO conversion at a 20 °C lower temperature on the former catalyst (10 nm) than on the other one. These authors concluded that catalysts with higher dispersion exhibit a higher activity for the CO methanation, while the lower dispersed catalyst tends to suppress the CO_2 conversion better. A similar particle size dependence of the activity was observed also by other groups [32,33], whereas other studies reported a decreasing activity with increasing Ru dispersion [21,34,35]. Gupta et al. [25,41] concluded from combined DRIFTS and kinetic measurements that the influence of the Ru dispersion on the methanation activity depends on the reaction temperature and suggested that different mechanisms are dominant below and above 220 °C. Only at temperatures below 220 °C, a dispersion dependent mechanism prevails.

The much higher activity of the Ru/zeolite compared to the Ru/Al_2O_3 catalyst observed in our study, both in terms of Ru mass-normalized rates and in turnover frequencies, is attributed to several reasons. Most directly, support effects arising from the different morphology (pore structure) and the different chemical properties of the zeolite surface (higher acidity) may contribute to the higher activity of the Ru/zeolite catalyst. In addition to changes in the surface chemistry, these effects may also modify the diffusion properties and thus the effective contact time [56]. Support effects were reported also in earlier studies [30,52]. Scirè et al. suggested that zeolites (in their work: ZSM-5) stabilize Ru in an oxidized, cationic form [30], while this is not or to a lesser extent possible for Al_2O_3 or SiO_2. The positive polarization of the Ru species was suggested to weaken the Ru-CO bond, via the resulting higher H_{ad} steady-state coverage, and thus to enhance the activity for the methanation reaction. Furthermore, the expected presence of very small Ru particles in the Ru/zeolite catalyst (<1 nm Ru particles) compared to the Ru/Al_2O_3 catalyst (2.5 nm Ru particles) may also affect the activity

of this catalyst via particle size effects, which would also modify the intrinsic activity described by the turnover frequency. Very small Ru nanoparticles would also be stabilized by the much higher surface area (410 $m^2\ g^{-1}$) of the Ru/zeolite catalyst compared to that of the Ru/Al_2O_3 catalyst (surface area 100 $m^2\ g^{-1}$). As long as the presence of very small Ru nanoparticles in the Ru/zeolite catalyst is not directly proven, but only indirectly concluded, this latter argument must remain tentative.

From measurements in idealized, semi-realistic and H_2O-rich semi-realistic reformate, we determined the apparent activation energies of the CO methanation reaction on the Ru/Al_2O_3 and the Ru/zeolite catalysts. The measurements were performed in the temperature range between 165 and 190 °C, after initial equilibration during 1000 min reaction at 190 °C (see Fig. 3a). To avoid irreversible changes of the catalyst, the reaction temperature was limited to 190 °C at maximum. The apparent activation energies obtained for the two catalysts are listed in Table 1 (Supplementary material). The measurements were performed first from high to low temperatures and then back to high temperatures again. For similar reaction conditions, the apparent activation energies are slightly lower on the Ru/zeolite catalyst than on the Ru/Al_2O_3 catalyst. In idealized reformate, the apparent activation energies are 90 ± 11 and 111 ± 10 kJ mol^{-1} for the Ru/zeolite and the Ru/Al_2O_3 catalyst, respectively. The values do not change significantly for reaction in semi-realistic and H_2O-rich semi-realistic reformate despite the lower activity of the Ru/zeolite catalyst in the latter reaction atmosphere (see also Section 3.3). The close similarity of the activation barriers points to a similar rate-limiting step for both catalysts and in different reaction mixtures. Comparable values for the activation energy were reported by Dalla Betta and Shelef [36] and Ekerdt and Bell [37] for reaction in a CO/H_2 mixture on Ru/Al_2O_3 and Ru/SiO_2 catalysts, respectively (Table 1, Supplementary material). In contrast, other groups reported higher values between 121 and 156 kJ mol^{-1} for reaction in CO/H_2 mixtures on differently loaded Ru/Al_2O_3 catalysts (see Table 1, Supplementary material) [16,22,57,58]. The spread in apparent activation energies is most likely due to the different reaction conditions in the different studies (see Table 1, Supplementary material). Finally, Panagiotopoulou et al. [22] reported that adding 15 kPa CO_2 to a CO/H_2 mixture lowers the activation energy on a 0.5 wt.% Ru/Al_2O_3 catalyst from 121 to 77 kJ mol^{-1}. This result contrasts our observation of a negligible variation in the activation energy upon variation of the reaction atmosphere. However, they measured the activation energy at higher temperatures (200–300 °C). The differences in the apparent activation energies in the presence of CO_2 in the reformate may indicate a change of the rate-limiting step above 190 °C.

The influence of the reactant concentration on the methanation reaction in idealized reformate was investigated by determining the reaction orders for CO and H_2 on both catalysts (Fig. 3b). This was done by stepwise varying the CO (H_2) partial pressure from 0.9 to 0.4 kPa (from 96.4 to 65 kPa), while keeping that of the second reactant constant (H_2: 96.4 kPa, CO: 0.6 kPa), and going back again to the initial partial pressure. Since the data agree closely, only the downwards runs are shown. The resulting CO reaction orders of −0.7 ± 0.1 and −0.5 ± 0.1 are of similar order of magnitude for the Ru/zeolite and the Ru/Al_2O_3 catalyst, respectively. For H_2, the Ru/zeolite catalyst (reaction order: 2.7 ± 0.2) shows a much more pronounced dependence of the activity on the H_2 concentration than the Ru/Al_2O_3 catalyst (reaction order: 1.0 ± 0.1). For comparison, Ekerdt and Bell [37] reported reaction orders of −1.1 and 1.8 for CO and H_2 on a Ru/Al_2O_3 catalyst at 240 °C and in idealized reformate (CO: 1 kPa, H_2: 1–20 kPa), respectively. The high reaction order of H_2 over of the Ru/zeolite catalyst may be a reason for its high activity, compared to the Ru/Al_2O_3 catalyst.

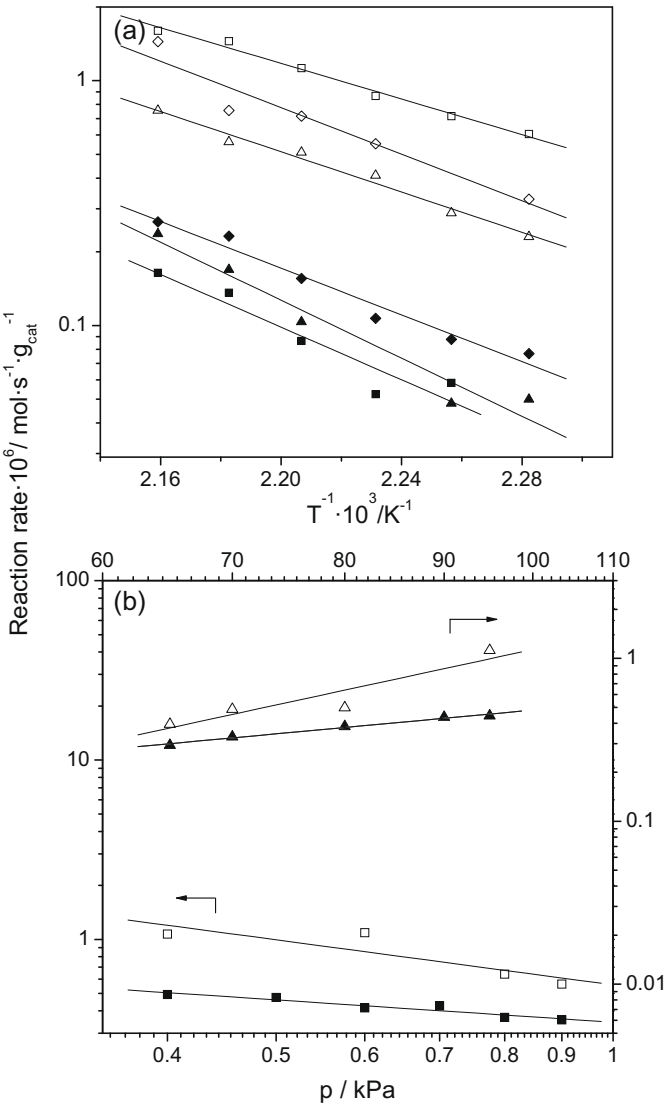

Fig. 3. (a) Arrhenius plot of temperature-dependent reaction rates after 1000 min methanation reaction on the Ru/Al_2O_3 (filled symbols) and the Ru/zeolite (open symbols) catalysts in different reformate gases: ▲, △: idealized reformate (0.6 kPa CO, 2.8 kPa N_2, rest H_2); ■, □: semi-realistic reformate (0.6 kPa CO, 2.8 kPa N_2, 15.5% CO_2, rest H_2); ♦, ◇: H_2O-rich semi-realistic reformate (0.6 kPa CO, 2.8 kPa N_2, 15 kPa CO_2, 5 kPa H_2O rest H_2). (b) Logarithmic plot of the partial pressure dependent reaction rates after 1000 min methanation reaction on the Ru/Al_2O_3 (■, △) and the Ru/zeolite (■, □) catalysts in idealized reformate (0.6 kPa CO, 2.8 kPa N_2, rest H_2): H_2 reaction order (□, △), CO reaction order (■, ▲).

3.3. DRIFTS measurements

In order to characterize the temporal evolution of the adsorbed surface species during the methanation reaction, we performed in situ IR measurements under the same reaction conditions as applied in the kinetic measurements described above (Fig. 2). Sequences of DRIFT spectra, recorded during 1000 min reaction on the Ru/zeolite and the Ru/Al_2O_3 catalyst in different reaction atmospheres, are shown in Figs. 4 and 5 (Fig. 4: idealized and CH_4-rich idealized reformate, Fig. 5: semi-realistic and H_2O-rich semi-realistic reformate). The spectra are split into 3 frequency ranges, the region of the OH (4000–3500 cm^{-1}, top left) and CH_x (3000–2800 cm^{-1}, top right) stretch vibrations in the top panels, respectively, and the spectral range between 800 and 2300 cm^{-1} including the CO stretch (2300–1900 cm^{-1}) and the OCO bending (1600–800 cm^{-1}) vibrations (bottom panel). The temporal evolution

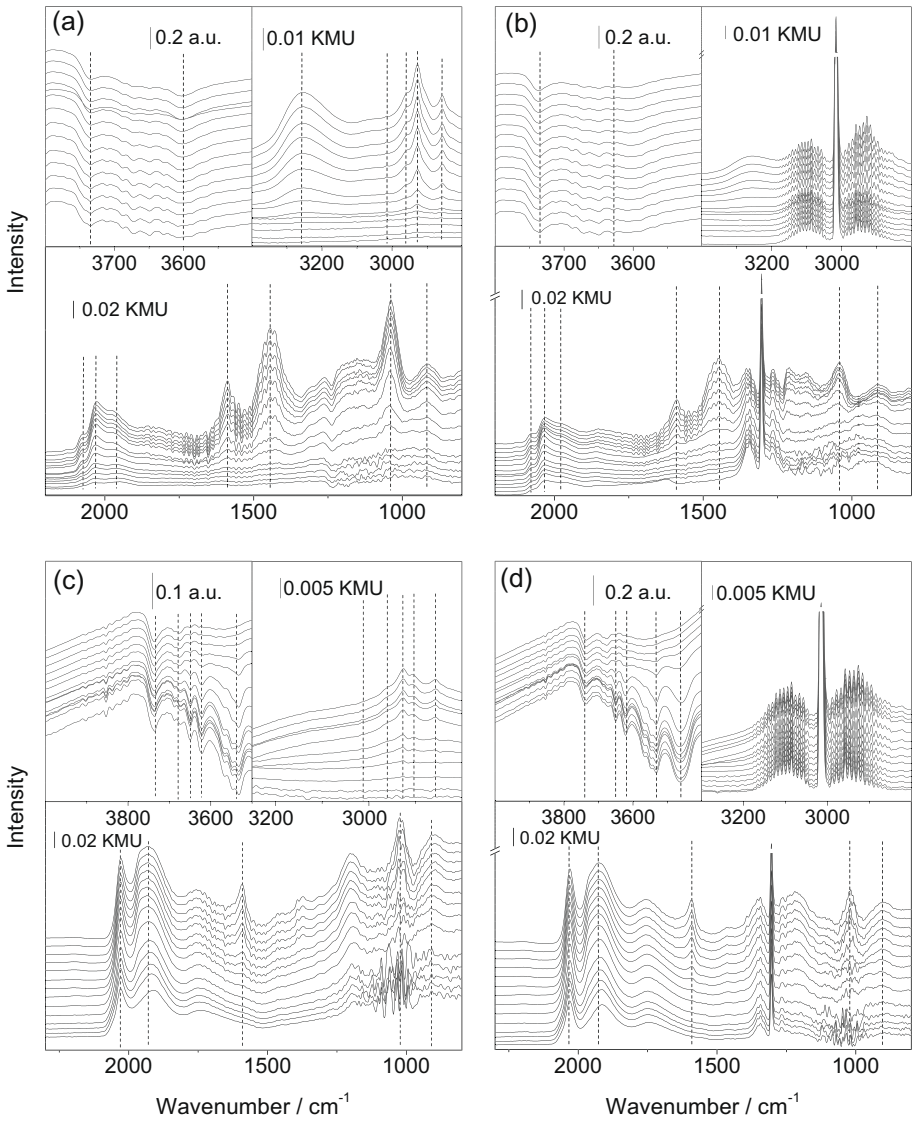

Fig. 4. Sequences of DRIFT spectra recorded during 1000 min methanation reaction on the Ru/zeolite catalyst at 190 °C in (a) idealized reformate (0.6 kPa CO, rest H_2) and (b) CH_4-rich idealized reformate (0.6 kPa CO, 4.5 kPa CH_4, rest H_2), and on the Ru/Al_2O_3 catalyst in (c) idealized reformate (0.6 kPa CO, rest H_2) and (d) CH_4-rich idealized reformate (0.6 kPa CO, 4.5 kPa CH_4, rest H_2). The spectra were recorded after 1, 2, 3, 5, 7, 15, 35, 105, 195, 345, 495, 645, 795, 945 min reaction time (from bottom to top).

of the different surface species was followed by the peak intensities, after normalization to similar background intensities directly aside the signals.

3.3.1. CO methanation

For reaction in idealized and CH_4-rich idealized reformate, we observe a fast build-up of signals in the CO region at 2075, 2036, and 1978 cm^{-1} on the Ru/zeolite catalyst, and at 2030 and 1940 cm^{-1} on the Ru/Al_2O_3 catalyst. On the latter catalyst, a dynamic equilibrium is reached after ~100 min, while on the Ru/zeolite catalyst the intensity decreased steadily. These signals are attributed to CO adsorbed on Ru [25,30,59–67]. The exact position depends on the pre-treatment of the catalyst and on the reaction conditions used in the experiment. The signal at 2036 cm^{-1} is commonly assigned to linearly adsorbed CO on Ru^0 [61,64,66,68]. In measurements on Ru/TiO_2 and Ru/Al_2O_3 catalysts, Londhe et al. [53] interpreted this signal as CO_{ad} linearly adsorbed on Ru, coadsorbed with and adjacent to O_{ad} species. Guglielminotti and Bond [64] observed a similar signal during the methanation reaction on a completely pre-reduced (only Ru^0 species) Ru/TiO_2 catalyst, and related this to linearly adsorbed CO on Ru^0. Measurements performed at different CO pressures revealed that the wave number of the linearly bound CO_{ad} species depends on the coverage, in good agreement with results of CO adsorption experiments on Ru (0 0 0 1) [68]. The signals at 1978 and 1940 cm^{-1} observed on the Ru/zeolite and the Ru/Al_2O_3 catalyst, respectively, were related to a bridge-bonded CO_{ad} adsorbed on Ru^0 [69]. Finally, the CO_{ad} related signal at higher wave numbers (2075 cm^{-1}), which is observed only on the Ru/zeolite catalyst, is assigned to dicarbonyl CO species adsorbed on very small Ru clusters or atoms on the support. These Ru species were proposed to result from oxidative disrupture of Ru–Ru bonds, and by some authors identified as oxidized Ru^{n+} sites [60,62,63,67]. In previous studies on the hydrogenation of CO over Ru/Al_2O_3 and Ru/SiO_2 catalysts, this signal was accompanied by a peak at 2135 cm^{-1} which can be detected at longer reaction times in our experiments as well. It should be noted, however, that the quantification of this signal is hindered by its overlap with the gas phase CO signal. Finally it should be noted that for CO interaction with the non-pretreated catalysts CO (both at room temperature and at 150 °C) adsorption was inhibited on the Ru/zeolite catalyst and showed similar features as during reaction on the Ru/Al_2O_3 catalyst, indicating that for

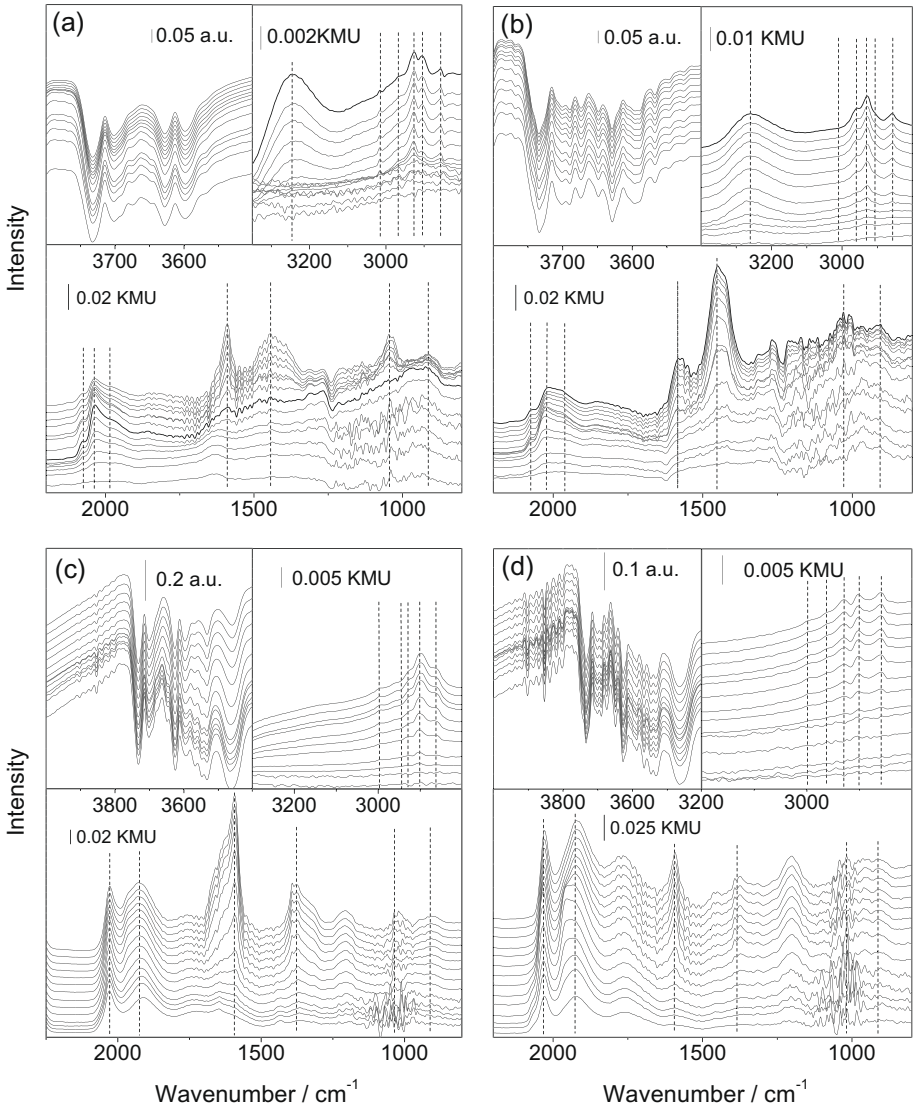

Fig. 5. Sequences of DRIFT spectra recorded during 1000 min methanation reaction on the Ru/zeolite catalyst at 190 °C in (a) semi-realistic reformate (0.6 kPa CO, 15.5 kPa CO_2, rest H_2) and (b) H_2O-rich semi-realistic reformate (0.6 kPa CO, 15.5 kPa CO_2, 5 kPa H_2O, rest H_2), and on the Ru/Al_2O_3 catalyst in (c) semi-realistic reformate (0.6 kPa CO, 15.5 kPa CO_2, rest H_2) and (d) H_2O-rich semi-realistic reformate (0.6 kPa CO, 15.5 kPa CO_2, 5 kPa H_2O, rest H_2). The spectra were recorded after 1, 2, 3, 5, 7, 15, 35, 105, 195, 345, 495, 645, 795, 945 min reaction time (from bottom to top).

the Ru/zeolite catalyst interaction with CO under these conditions is not sufficient to initiate surface reduction. After reactive pretreatment, the CO adsorption behavior was similar as during reaction.

In the OH region, two peaks at 3630 and 3740 cm^{-1} are observed on the Ru/zeolite catalyst, which we relate to isolated OH_{ad} groups on the support (Fig. 4) [70,71]. They are visible already at the beginning of the reaction and do not change significantly in intensity during the reaction. On the Ru/Al_2O_3 catalyst, three additional OH_{ad} signals are present at 3650, 3620, and 3540 cm^{-1} during the reaction. With ongoing reaction, the intensity of the peak at 3740 cm^{-1} remains constant, whereas that of the other four signals decreases.

In the OCO region, peaks at 1589, 1442, 1044, and 915 cm^{-1} appear after about 100 min reaction on the Ru/zeolite catalyst (Fig. 4). They continuously increase in intensity and do not reach a steady-state during the reaction time. On the Ru/Al_2O_3 catalyst (Fig. 4), the OCO region exhibits peaks at 1587, 1374, 1040, and 915 cm^{-1}, which appear after 35 min reaction and steadily increase in intensity. According to previous studies, peaks at ~1585–1590 and 1374 cm^{-1} result from the antisymmetric and symmetric bending vibrations of surface formates, respectively [36,40,64,72], which can be formed during the methanation reaction by reaction of CO with water. The corresponding C–H vibration, which was reported to appear at ~2902 cm^{-1}, appears here at ~2905 cm^{-1} (see below). As discussed in earlier studies, these formate species are at least mainly located on the Al_2O_3 support [73], although additional adsorption on the Ru nanoparticles can not be ruled out. During methanation on Ru/TiO_2 and Ru/Al_2O_3 catalysts, Gupta et al. [40] and Dalla Betta and Shelef [36] also detected a peak at 1440 cm^{-1}, which they assigned to the OCO bending vibration of a surface carbonate species. In the present work, a comparable signal is only detected on the Ru/zeolite catalyst at 1442 cm^{-1}. Comparing with earlier methanol adsorption experiments on a $Cu–ZnO/Al_2O_3$ catalyst [74], the signal at 1040 cm^{-1} may be related to a methoxy or methanol species adsorbed on the support. It is usually accompanied by a peak at 1085 cm^{-1} [74], which we cannot observe here. Possibly, the latter peak is obscured by the intense signal at 1040 cm^{-1}. The peak at 915 cm^{-1} is tentatively assigned to a deformation mode of $CH_{2,ad}$

species adsorbed on the Al_2O_3 support [74], pointing to possible CH_x chain growth on the support during the reaction [74]. Adding CH_4 to the idealized gas mixture, three additional peaks appeared at 1305 cm^{-1}, 1344, and 1264 cm^{-1}, which represent the Q, P, and R branches of gas phase methane [66].

The CH spectral region (Figs. 4 and 5) shows the typical $CH_{x,ad}$ signals at 3015, 2958, 2927, and 2857 cm^{-1}, arising from CH_4, $CH_{3,ad}$, and the symmetric and asymmetric $CH_{2,ad}$ vibrations on the two catalysts [30,37,66]. These surface species start to grow in after about 5 min reaction time. They increased further until reaching a steady-state after 340 and 1000 min reaction on the Ru/Al_2O_3 and Ru/zeolite catalyst, respectively. The shoulder at ~2905 cm^{-1} can be assigned to the CH vibration of a surface formate [36,40]. During reaction in the CH_4-rich reformate, the $CH_{x,ad}$-related signals are obscured by the strong CH_4 signal in the range of ~2800 to ~3200 cm^{-1} [66].

Comparing the reaction in idealized (Fig. 4) and in CH_4-rich idealized reformate (Fig. 4), we find no major differences in the surface species. The situation is very different, when the adlayer and its evolution with time are compared for the Ru/Al_2O_3 and the Ru/zeolite catalyst. Here we find a number of differences, with the major ones being:

(i) On the Ru/zeolite catalyst, the intensity of the signal at 2036 cm^{-1}, which is related to Ru–CO, decays slowly with time, and this decay agrees perfectly with the slight deactivation of the catalysts with time (Fig. 2). For the Ru/Al_2O_3 catalyst, the signal is stable, and this catalyst is essentially stable against deactivation.
(ii) The CO_{ad} signal on oxidized Ru at 2075 cm^{-1} is observed only on the Ru/zeolite catalyst and absent on the Ru/Al_2O_3 catalyst.
(iii) On the Ru/Al_2O_3 catalyst, additional signals related to OH_{ad} groups are observed at 3650 and 3550 cm^{-1}.
(iv) The build-up of surface carbonates is negligible on the Ru/Al_2O_3 catalyst, whereas on the Ru/zeolite catalyst surface carbonate growth is strong.

The close correlation in the time dependences of the CO methanation activity and the time evolution of the signal intensity at 2036 cm^{-1} indicates that the same Ru^0 sites active for CO adsorption are also active for the methanation reaction, making the number of Ru^0 surface sites crucial for the reaction. The CO_{ad} on Ru^0 sites visible in IR may be directly involved in the reaction, but this is not necessarily required, and, though unlikely, they may also act as spectator species. This correlation and therefore also the mechanistic conclusion are true for both catalysts.

Gupta and Tripathi had suggested that at lower temperatures (<220 °C) Ru^{n+}–$(CO)_m$ species represent the active species [41]. Other groups [66,72,75], however, have questioned this proposal because of the rather weak adsorption of CO on Ru^{n+} sites and the resulting low steady-state coverage of these species under reaction conditions. Furthermore, the weak interaction between Ru^{n+} sites and CO is likely to result in a less pronounced weakening of the C–O bond compared to bonding on Ru^0 sites, due to a lower population of the antibonding $2\pi^*$ orbital of the CO_{ad}. Contributions from oxidized Ru^{n+} sites and Ru^{n+}–CO species can not be ruled out from the present data, but are also not supported by them.

Another difference between the Ru/Al_2O_3 and the Ru/zeolite catalyst lies in the stability of the Ru nanoparticles. For the Ru/zeolite catalyst, we observed a decrease by ca. 20% of the signal at 1990 cm^{-1}, which is related to bridge-bonded CO_{ad} on Ru^0, after 105 min on stream, and a similar intensity decrease was observed also for the other Ru–CO signals. This can be explained in two ways, either by sintering or reductive agglomeration of the Ru particles, which was also suggested by Solymosi and Raskó [62], or by partial covering of the Ru surface by adsorbates such as $CH_{x,ad}$ species. The decay in Ru surface area active for CO adsorption is not correlated with a decrease or increase of the IR signals related to other surface species (e.g., $CH_{x,ad}$, surface formates or surface carbonates). During the methanation reaction on the Ru/Al_2O_3 catalyst, the Ru^0–CO related signals are stable after about 100 min.

From the absence of any correlations between the temporal evolution of surface formates and surface carbonates on the one hand and the methanation activity on the other hand we conclude that the reaction is not dominated by the reaction/decomposition of either of these surface species.

The relative intensities and the temporal evolution of the $CH_{x,ad}$-related intensities differ widely on both catalysts, with the relative intensities being higher on the Ru/zeolite catalyst. On the same catalyst, the signal intensities and hence the coverages of the related surface species reach a dynamic equilibrium situation after about 1000 min, while on the Ru/Al_2O_3 catalyst this occurs after 340 min. Most simply this is explained by either a much slower build-up of the $CH_{x,ad}$ species on the Ru/zeolite catalyst or their faster decomposition on the Ru/Al_2O_3 catalyst. This agrees also with the lower steady-state coverage of these species on the Ru/Al_2O_3 catalyst. In addition, due to the higher surface area of the Ru/zeolite support, more adsorption sites for the $CH_{x,ad}$ species are expected. The $CH_{x,ad}$ species were suggested as intermediates in the methanation reaction [37,38,76], which was described already in the introduction, and will be discussed in more detail in the last section (Section 3.3.3).

The role of surface formates and carbonates, which are formed by reaction of CO with H_2O during the methanation reaction, is not clear yet. Since carbonates are only present on the Ru/zeolite catalyst, it is more likely that these species represent reaction side products. Regarding the role of the surface formates, several groups proposed them to be side products of the reaction [36,37,40]. Prairie et al. [23] suggested that during CO_2 methanation surface formates may serve as a reversible CO reservoir. The role of the surface formates will be discussed in more detail in Section 3.3.3.

3.3.2. Selective methanation

Similar in situ DRIFTS experiments as described above were performed in semi-realistic and in H_2O-rich semi-realistic reformate, containing both CO and CO_2 (Fig. 5). The general characteristics of the resulting spectra are rather similar to those obtained in idealized reformate (Fig. 4), with the following differences:

(i) The presence of CO_2 leads to overtone signals of CO_2 in the OH region on both catalysts; therefore the intensities related to the OH groups could not be evaluated.
(ii) The tendency for surface formate and/or carbonates formation is more pronounced (higher steady-state coverage) on both catalysts in these reaction atmospheres compared to reaction in CO_2-free idealized reformates (Section 3.3.1).
(iii) In H_2O-rich semi-realistic atmosphere, a signal at 2075 cm^{-1} (shoulder) is detected also on Ru/Al_2O_3, which was not observed in the other gas-mixtures. It is attributed to CO_{ad} on oxidized Ru^{n+} species.
(iv) For the Ru/zeolite catalyst, the temporal evolution of the CO_{ad} species changes in the presence of H_2O (H_2O-rich semi-realistic reformate) compared to all H_2O free reaction mixtures, leading to much lower CO_{ad} coverages during the reaction.

It is interesting to note that among the different additional components only water has a negative effect on the adsorption behavior of CO on Ru (Fig. 5b), and only on the Ru/zeolite catalyst. In the presence of water vapor, the intensity of linear and bridge-bonded CO_{ad} species on Ru^0 decreased compared to reaction in water-free atmo-

sphere. This may be due to the blocking of adsorption sites by adsorbed water or, alternatively, by Ru (surface) oxidation. The CO_{ad} species adsorbed on oxidized Ru, however, does not seem to be influenced much by water addition, and the total amount of Ru^{n+}–CO species stays the same. Together with the lower intensity in the Ru^0–CO signal, also the CO methanation activity is lower in H_2O-rich atmosphere than in H_2O-free atmosphere, and both of them decrease slowly with time. On the other hand, for the Ru/Al_2O_3 catalyst, the presence of water in the reaction atmosphere leads to a signal at 2075 cm^{-1} (formation of a small shoulder), while neither the intensity of the 2036 cm^{-1} signal nor the CO methanation activity are lower in the presence of H_2O than in (H_2O-free) semi-realistic reformate. The observed close correlation between Ru^0–CO signal intensity and the CO methanation activity also upon changing to a H_2O-rich gas mixture provides further support for our above conclusion that the activity of the Ru catalysts is closely correlated with the number of accessible Ru^0 sites in the reaction.

The combined addition of CO_2 and water has a direct influence on the formation of surface carbonate and/or formate species on both catalysts. The intensity of the signal at ~1590 cm^{-1}, which is related to surface formate species, grows very fast on the Ru/zeolite catalyst and reaches an even higher value than that of the surface carbonate-related peak at ~1440 cm^{-1}, while this is opposite in idealized reformate. The same trends are observed for the Ru/Al_2O_3 catalyst. Prairie et al. [23] had shown that CO_2 and H_2 react to a formate species on Ru/TiO_2 and Ru/Al_2O_3 catalysts, which explains the increased tendency for surface formate formation of our catalysts upon CO_2 addition. The addition of water, on the other hand, suppresses the build-up of formates. Most likely, this proceeds via an enhanced formate decomposition, since a dynamic equilibrium is reached after 200 min. Marwood et al. [77] observed similar trends during the CO_2 methanation reaction, finding a strong decrease of the surface formate species with increasing water concentration. This may be due to blocking of adsorption sites by OH_{ad} groups or due to water-induced faster decomposition of the surface formates. Finally, the build-up of the surface carbonates (1440 cm^{-1}) increases on the Ru/zeolite catalyst when adding water to the gas-mixture (Fig. 5b).

Comparing the temporal evolution of the CO methanation activity (Fig. 2) with the results of the above DRIFTS experiments reveals a distinct correlation between the time dependence of the activity and the intensities/concentrations of the Ru^0–CO species. The kinetic measurements show, after a subtle initial increase during the first ~50 min, a slow decay of both the methanation activity and the Ru^0–CO signal intensity with time, by about 20% over 1000 min on stream, whereas for the Ru/Al_2O_3 catalyst, both remain constant with time. Furthermore, the lower activity of the Ru/zeolite catalyst in H_2O-rich semi-realistic reformate relative to the other gas mixtures goes along with a lower Ru^0–CO signal intensity. The close correlation led us to propose that the number of active sites is closely related to the number of Ru^0 sites, and that they are likely to represent active sites in the methanation reaction on both catalysts (see earlier discussion in this section).

The surface formates and carbonates increase steadily in intensity, and the $CH_{x,ad}$ species seem to saturate between 900 and 1000 min on the Ru/zeolite catalyst and after 340 min on the Ru/Al_2O_3 catalyst, respectively. Hence, there is no simple correlation between the intensity and concentration behavior of any of these species and the methanation activity. Therefore it is not likely that the reaction is dominated by the reaction/decomposition of any of these surface species, which will be discussed in more detail in the following section.

3.3.3. Transient experiments

After following the build-up of the surface species during the methanation reaction in adsorption transients in different reaction atmospheres on the Ru/Al_2O_3 and Ru/zeolite catalysts in the last section, we evaluated the stability of these surface species in idealized reformate in decomposition transients. This was done by following their transient behavior upon replacing CO in the reaction atmosphere by N_2 after 1000 min reaction, i.e., by changing from a CO/H_2 mixture to a N_2/H_2 atmosphere. The temporal evolution of the signal intensities related to $CH_{x,ad}$, surface formate and surface carbonate species was evaluated from a sequence of DRIFT spectra recorded upon $CO/H_2 \rightarrow N_2/H_2$ exchange.

The resulting changes in the adlayer on the Ru/zeolite and on the Ru/Al_2O_3 catalyst are illustrated in Fig. 6. On the Ru/zeolite catalyst (Fig. 6a), the CO_{ad}-related signals vanish within the first 3 min. Also on the Ru/Al_2O_3 catalyst, the CO_{ad} signal decreases within 3 min, but does not disappear completely. Even 1000 min after the exchange, two peaks at 2040 and 1960 cm^{-1} are present, which indicate the presence of linear- and bridged-bonded CO_{ad} on Ru^0. The rapid decay of the CO_{ad}-related intensity is explained by CO_{ad} reaction, e.g., with the H_2 present in the gas phase, and by CO_{ad} desorption. The reason for the persistence of the remaining CO_{ad} signals is still unclear, small signals were observed even after treatment at 250 °C in N_2.

Following the intensities related to surface formates, surface carbonates, $CH_{2,ad}$ and $CH_{3,ad}$ at 1590, 1440, 2927, and 2956 cm^{-1} on the Ru/zeolite catalyst, respectively, we find that all of these adspecies decrease in concentration with time. The stability of these species follows the order surface carbonate > surface formate > $CH_{3,ad} \geqslant CH_{2,ad}$. Since the initial rate of the decrease in intensity is low for the surface carbonates and formates, and certainly well below the methanation rate [78], we suggest that these species are side products. The $CH_{x,ad}$ species adsorbed on the support of the catalyst (they are formed also on the pure zeolite) show the highest relative decrease in intensity, decreasing to 30% of the value after 1000 min reaction.

On the Ru/Al_2O_3 catalyst, the intensities of the adsorbed surface species decrease much more rapidly than on the Ru/zeolite catalyst. Within the first 45 min, the signals related to surface formates and $CH_{x,ad}$ species decay to almost their final intensity, and then remain essentially constant. The intensity loss of the $CH_{x,ad}$-related signals (2958, 2927, 2857 cm^{-1}) is about 80%, which is even more pronounced than on the Ru/zeolite catalyst, while the formate intensities decrease by about 60% relative to the initial intensity (after 1000 min reaction). Surface carbonates were not formed on this catalyst during the reaction. Finally, the signals of the methoxy species and of the $CH_{2,ad}$ species at 1040 and 915 cm^{-1}, respectively, increase rather than decrease in intensity upon changing from $CO/H_2 \rightarrow N_2/H_2$. This increase in methoxy species, which probably result from other adsorbed surface species such as surface formates, indicates that these are not part of the reaction chain. The growing intensity of the 915 cm^{-1} signal is attributed to accumulation of $(CH_2)_x$ chains on the surface [74].

Ekerdt and Bell suggested that $CH_{x,ad}$ species are intermediates in the methanation reaction [37]. They concluded this from transient isotope-labeling IR experiments. It should be noted, however, that, due to the lacking quantification of their IR intensities it is not clear whether the $CH_{x,ad}$ species observed spectroscopically act as reaction intermediate in the dominant reaction pathway or whether they represent a (little reactive) spectator species. Yamasaki et al. [38] also investigated the reaction pathway of CO and hydrogen on a Ru/SiO_2 catalyst. They used an indirect method proposed by Wexler [79] for quantifying the coverages of the adsorbed methylene and methyl groups (see also Section 1), and calculated the mean chain length of adsorbed hydrocarbon chains from the ratio of these groups. From transient IR experiments, they proposed a complex mechanism for the CO methanation reaction, where $CH_{x,ad}$ species act as reaction intermediates and CH_4 formation proceeds via formation and decomposition of adsorbed hydrocarbon chains

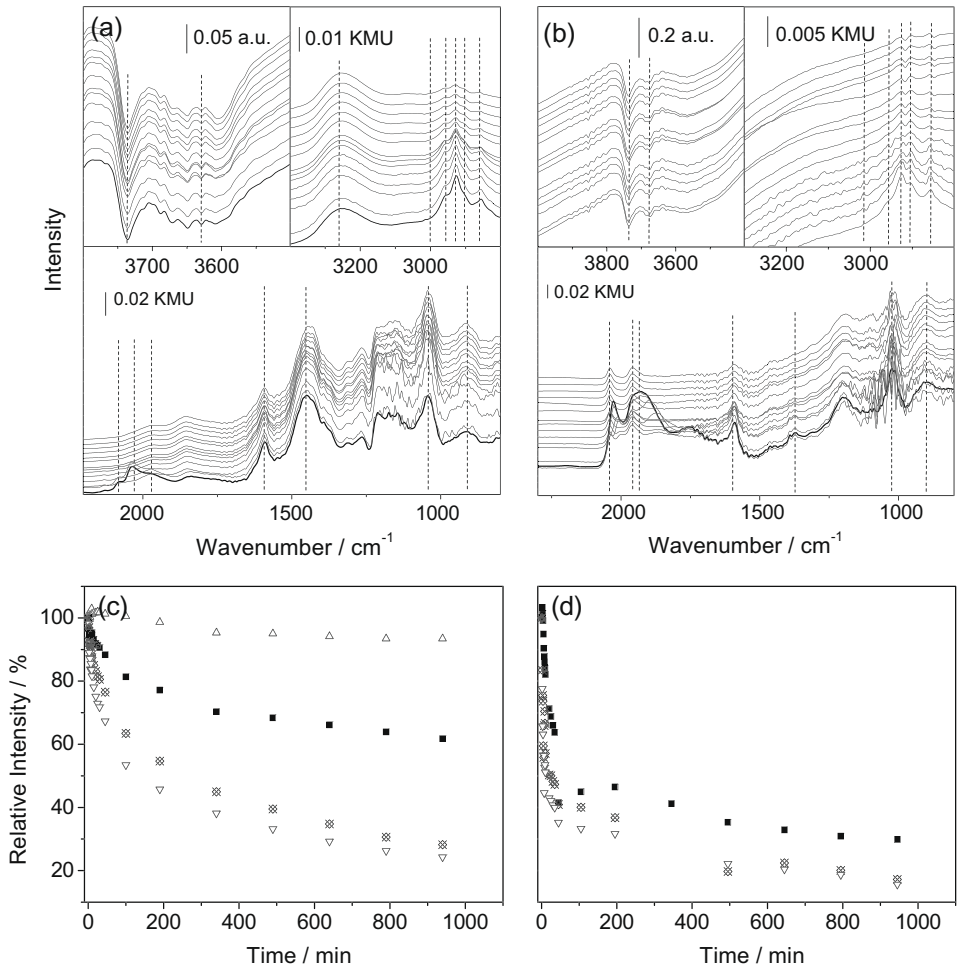

Fig. 6. Upper panels: sequences of DRIFT spectra recorded upon exchanging CO by N_2 in the reaction gas mixture on (a) the Ru/zeolite catalyst and (b) the Ru/Al_2O_3 catalyst at 190 °C in idealized reformate (0.6 kPa CO, rest H_2) after 1000 min reaction. The spectra were recorded after: 0 min (end of the 1000 min reaction), 1, 2, 3, 5, 7, 15, 35, 105, 195, 345, 495, 645, 795, and 945 min (from bottom to top). Bottom panels: relative intensities of the $CH_{x,ad}$ surface formate and surface carbonate related signals at 2958, 2927, 2857, 1590 cm^{-1} and at 1440 cm^{-1} during the transient experiment on the Ru/zeolite (c) and the Ru/Al_2O_3 (d) catalyst. △: Surface carbonate, ■: surface formate, ▽: $CH_{2,ad}$, ▨: $CH_{3,ad}$.

[38]. Since, however, the authors could not demonstrate that the decomposition rate of the hydrocarbon chains under steady-state conditions corresponds quantitatively to the CH_4 formation rate, definite proof for this proposal is still missing.

For more quantitative information on these aspects, in particular on the correlation between decomposition of the $CH_{x,ad}$ species and CH_4 formation rate on the Ru/zeolite catalyst, we performed a similar transient experiment as shown in Fig. 6, but following the decay of the CH_4 formation rate by a mass spectrometer. The resulting CH_4 formation transient, recorded upon changing from a CO/H_2 mixture to a Ar/H_2 mixture under similar reaction conditions as before (see Fig. 6), is plotted in Fig. 7. Upon changing from the reaction mixture to the Ar/H_2 mixture, the formation of CH_4 decreases rapidly and reaches the background level within 3–4 min. For comparison, the decay of the IR intensities related to $CH_{2,ad}$ and $CH_{3,ad}$ proceeds on a much longer time scale (Fig. 6). After 100 min exposure to N_2/H_2, the related signals show still more than 50% of their initial intensity, and the further decay of the $CH_{x,ad}$ related signals is rather slow. Even after 1000 min exposure to a N_2/H_2 mixture, the intensity of these signals is still around 25% of the initial value. Hence, hydrogenation of the $CH_{x,ad}$ species visible in IR to $CH_{4,ad}$ and its subsequent rapid desorption can not represent the rate limiting step for CH_4 formation. The question for the rate-limiting step and the nature of the reaction intermediate in the dominant reaction pathway is, at least from the experimental point of view, still open. Based on the present data, the $CH_{x,ad}$ species visible in the IR spectra represent spectator species, whose reaction to CH_4 is much slower than required for explaining the observed CH_4 formation rate. Therefore, the formation and hydrogenation of the $CH_{x,ad}$ species visible in IR cannot represent the

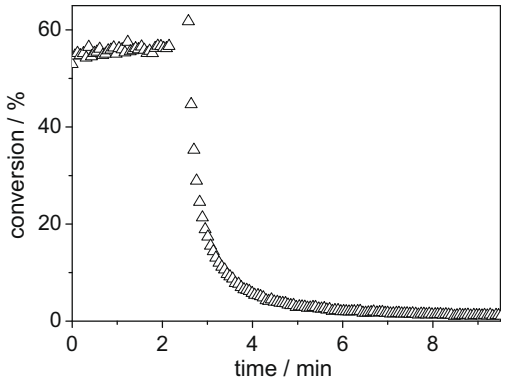

Fig. 7. Transient activity measurement of Ru/zeolite upon exchange of CO by Ar under idealized reaction conditions (0.6 kPa CO, rest H_2) after 1000 min reaction at 190 °C; △: CH_4 conversion.

dominant reaction pathway. This conclusion agrees well with recent predictions based on density functional theory calculations [44–46], which favor a reaction pathway via formyl formation rather than via C–O bond splitting and subsequent hydrogenation. Based on the similar trends in the DRIFTS transients shown in Fig. 6, we expect that these mechanistic conclusions are valid for both Ru catalysts, although the removal of the adsorbed $CH_{x,ad}$ species is faster on the Ru/Al_2O_3 catalyst than on the Ru/zeolite catalyst.

4. Summary

We have investigated the selective methanation of CO in different CO_2-containing reformates on a 2.2 wt.% Ru/zeolite catalyst and, for comparison, on a 5 wt.% Ru/Al_2O_3 catalyst by temperature-screening measurements, kinetic measurements under differential reaction conditions and by transient in situ DRIFTS and mass spectrometric measurements. The latter experiments focused on the build-up of adsorbed surface species during the reaction and their decomposition upon replacing the CO/H_2 mixture in the reaction gas by a N_2/H_2 or a Ar/H_2 mixture. These measurements led to the following results:

1. Temperature-dependent conversion measurements showed that both catalysts are active for the selective methanation reaction. Under present reaction conditions, full conversion of CO was achieved at 200 °C and 230 °C for the Ru/zeolite and the Ru/Al_2O_3 catalyst, respectively, in idealized reformate. The addition of water and methane did not influence the CO methanation activity on the Ru/zeolite catalyst and caused only minor changes in the CO conversion on the Ru/Al_2O_3 catalyst. The addition of CO_2 (CO_2-rich idealized reformate) led to an acceleration of the reaction on the Ru/zeolite catalyst, where complete CO conversion (T_{100}) was reached now at 190 °C. On that catalyst, CO_2 methanation started after complete CO conversion, and the selectivity for CO conversion remained above 85% over a temperature range of 40 °C. On the Ru/Al_2O_3 catalyst, CO_2 conversion started at 200 °C, where CO was still left in the reformate. With increasing temperature, both CO and CO_2 are converted and at full CO conversion the selectivity for CO methanation has decreased to 48% under present reaction conditions. In the absence of CO, in CO_2/H_2 mixtures, the CO_2 conversion exhibits similar conversion characteristics as the CO conversion on the Ru/Al_2O_3 catalyst. On the Ru/zeolite catalyst, in contrast, the onset of CO_2 conversion is shifted to lower temperature (170 °C), and the subsequent increase in conversion is rather slow, reaching full conversion only at 410 °C. The latter behavior points to a kinetic hindrance in CO_2 methanation, in the absence and presence of CO.
2. Kinetic measurements performed under differential conditions exhibited a ~10 to ~20 times higher Ru mass-normalized reaction rate over the Ru/zeolite catalyst compared to the Ru/Al_2O_3 catalyst. For the inherent activity, expressed by the turnover frequency, the differences are even higher with factors between 10 and 30, which correspond to TOFs between 67 and 135 s^{-1} on the Ru/zeolite catalyst, depending on the reaction atmosphere. Temperature-dependent measurements, performed in idealized reformate after 1000 min on stream in the range 190–160 °C, revealed comparable apparent activation energies for both catalysts under these conditions, pointing to a similar rate-limiting step on both catalysts. On the Ru/Al_2O_3 catalyst, reaction orders of −0.5 and 1.0 were obtained for CO and H_2, respectively. Higher reaction orders of −0.7 and 2.7 for CO and H_2, respectively, were observed on the Ru/zeolite catalyst. One may speculate that the high value for the reaction order of H_2 is linked to the high activity of this catalyst.
3. In situ IR (DRIFTS) measurements showed that exposing the catalysts to different reaction mixtures under reaction conditions leads to the immediate adsorption of linearly- and bridge-bonded CO_{ad} species on Ru^0 sites on both catalysts. On the Ru/zeolite catalyst, an additional signal appeared at higher frequency (2075 cm^{-1}), which is attributed to CO_{ad} on Ru^{n+} sites. This species was not observed on the Ru/Al_2O_3 catalyst in H_2O-free reaction atmospheres, whereas in the presence of water a small shoulder of this signal developed, due to the more oxidizing reaction conditions. In addition, on both catalysts we observed the build-up of surface formates and $CH_{x,ad}$ species, while surface carbonates were formed on the Ru/zeolite catalyst only. Thus, the presence of a Ru^{n+}–CO species and the observation of an additional OH_{ad} signal are the most striking differences in the IR spectra between the two catalysts.
4. The temporal evolution of the DRIFTS signals related to the different adsorbed CO surface species differs significantly between the two catalysts. On the Ru/zeolite catalyst, the intensity of the CO_{ad}-related signals passes through a maximum after 100 min reaction, whereas for the Ru/Al_2O_3 a steady-state situation is reached at the same time. The signals related to surface formates and carbonates do not saturate during 1000 min on stream, those related to $CH_{x,ad}$ species reach a dynamic equilibrium after about 1000 min on the Ru/zeolite catalyst and after 340 min on the Ru/Al_2O_3 catalyst, respectively.From the close correlation between Ru^0–CO signal intensity and the methanation activity on both catalysts, which is observed in the time-dependent behavior and also when comparing different gas mixtures, we propose that the activity in the methanation reaction is determined by the number of accessible Ru^0 sites on the two catalysts. Ru^0–CO species may act as active sites and active species, but other species adsorbed on Ru^0 sites may be possible as well. On the other hand, the absence of such correlations between surface formates and surface carbonates and methanation activity indicates that the reaction is not dominated by the reaction/decomposition of either of these surface species.
5. Changing from CO-containing to CO-free reaction atmosphere after 1000 min on stream in idealized reformate, surface formates and $CH_{x,ad}$ species disappear with time on both catalysts. The initial rate of decomposition, however, differs significantly from the steady-state reaction rate. Therefore, the reaction between the $CH_{x,ad}$ species visible by IR and hydrogen can not represent the rate-limiting step in the dominant reaction pathway. The same experiment performed with a mass spectrometer shows that CH_4 is not produced anymore after 3 min upon switching to an Ar/H_2 mixture, providing further support for the above conclusion. The signals representing ($-CH_2-$) chain groups were growing even after replacement of CO, and are therefore identified as side products.

The kinetic and DRIFTS measurements showed that both Ru catalysts are active and selective for the CO methanation even at low temperatures (190 °C). Using zeolite as support material, the Ru catalyst shows significantly higher activity and selectivity, probably due to specific interactions between the more acidic support and the Ru nanoparticles and via the stabilization of very small metallic and oxidic Ru particles, which result in pronounced modifications of the intrinsic Ru surface activity described by turnover frequencies. The higher surface area of the zeolite support may further contribute to the better performance of this catalyst.

Acknowledgments

We are grateful to the Süd-Chemie AG for providing the Ru/zeolite catalyst. Furthermore, we want to acknowledge H.G. Anfang (Süd-Chemie AG) for extensive discussions and Y.-F. Han (ICES

Institute of Chemical and Engineering Sciences, Singapore) for his contributions in the initial measurements of the CO and CO_2 methanation reaction on the Ru/Al_2O_3 catalyst. We thank V. Hagen (Lehrstuhl für Technische Chemie, Ruhr Universität Bochum) and D. Widmann (Institute of Surface Chemistry and Catalysis, Ulm University) for the H_2 adsorption measurements, L. Kroner (Institute of Nano- and Microstructured Materials, Ulm University) for the XRD measurements and F. Krumeich (EMEZ – Electron Microscopy ETH Zürich) for TEM/STEM imaging.

Appendix A. Supplementary material

Supplementary data associated with this article can be found, in the online version, at doi:10.1016/j.jcat.2009.10.025.

References

[1] W. Lubitz, W. Tumas, Chem. Rev. 107 (2007) 3900.
[2] S. Kawatsu, J. Power Sources 71 (1998) 150.
[3] D.L. Trimm, Z.I. Önsan, Catal. Rev. 43 (2001) 31.
[4] J.R. Rostrup-Nielsen, K. Aasberg-Petersen, in: W. Vielstich, H.A. Gasteiger, A. Lamm (Eds.), Fuel Cell Technology and Applications, first ed., vol. 3, Wiley, Chichester, 2003 (Chapter 14).
[5] J. Sehested, S. Dahl, J. Jacobsen, J.R. Rostrup-Nielsen, J. Phys. Chem. B 109 (2005) 2432.
[6] R.M. Navarro, M.A. Pena, J.L.G. Fierro, Chem. Rev. 107 (2007) 3952.
[7] D.R. Palo, R.A. Dagle, J.D. Holladay, Chem. Rev. 107 (2007) 3992.
[8] S. Gottesfeld, T.A. Zawodzinski, in: R.C. Alkire, H. Gerischer, D.M. Kolb, C.W. Tobias (Eds.), Advances in Electrochemical Science and Engineering, vol. 5, Wiley-VCH, Weinheim, 1997.
[9] US Department of Energy, Multi-Year Research, Development and Demonstration Plan: Planned Program Activities for 2005–2015, US Department of Energy Ref Type: Electronic Citation, 2009.
[10] W. Vielstich, in: A.J. Bard, M. Stratmann, E.J. Calvo (Eds.), Encyclopedia of Electrochemistry – Interfacial Kinetics and Mass Transport, vol. 2, VCH, Weinheim, 2003.
[11] J.R. Ladebeck, J.P. Wagner, in: W. Vielstich, A. Lamm, H.A. Gasteiger (Eds.), Handbook of Fuel Cells – Fundamentals Technology and Applications, vol. 3, Wiley, Chichester, 2003.
[12] L. Shore, R. Farrauto, in: W. Vielstich, H.A. Gasteiger, A. Lamm (Eds.), Fuel Cell Technology and Applications, first ed., vol. 3, Wiley, Chichester, 2003 (Chapter 18).
[13] M. Echigo, T. Tabata, J. Chem. Eng. Jpn. 37 (2004) 75.
[14] L. Caldwell, in: Report 660 5 2, Council for Scientific and Industrial Research, Republic of South Africa, 1980.
[15] C.H. Bartholomew, Catal. Lett. 7 (1990) 303.
[16] S.S. Ranghava, R.C.E.H. Amirali, I&EC Process Design and Development, 1969, p. 482.
[17] G.A. Mills, F.W. Steffgen, Catal. Rev. Sci. Engin. 8 (1974) 159.
[18] M.A. Vannice, J. Catal. 3 (1974) 449.
[19] M.S. Batista, E.I. Santiago, E.M. Assaf, E.A. Ticianelli, J. Power Sources 145 (2005) 50.
[20] Y. Men, G. Kolb, R. Zapf, V. Hessel, H. Löwe, Catal. Today 125 (2007) 81.
[21] Z. Kowalczyk, K. Stolecki, W. Rarog-Pilecka, E. Miskiewicz, E. Wiczkowska, Z. Karpinski, Appl. Catal. A 342 (2008) 35.
[22] P. Panagiotopoulou, D.I. Kondarides, X.E. Verykios, Appl. Catal. A 344 (2008) 45.
[23] M.R. Prairie, A. Renken, J.G. Highfield, K.R. Thampi, M. Grätzel, J. Catal. 129 (1991) 130.
[24] F. Solymosi, A. Erdöhelyi, M. Kocsis, J. Chem. Soc. Faraday Trans. 77 (1981) 1003.
[25] N.M. Gupta, V.P. Londhe, V.S. Kamble, J. Catal. 169 (1997) 423.
[26] J. Zhang, M.B. Vukmirovic, K. Sasaki, U.N. Anand, M. Mavrikakis, R. Adzic, J. Am. Chem. Soc. 127 (2005) 12480.
[27] A.R. Dagle, Y. Wang, G.-G. Xia, J.J. Strohm, J. Holladay, D.R. Palo, Appl. Catal. A 326 (2007) 213.
[28] D.J. Elliott, J.H. Lunsford, J. Catal. 57 (1978) 11.
[29] P.A. Jacobs, H.H. Nijs, J.J. Verdonck, J.E. Uytterhoeven, in: Symposium on Advances in Fischer–Tropsch Chemistry, Anaheim Meeting, American Chemical Society, 1978, p. 469.
[30] S. Scirè, C. Crisafulli, R. Maggiore, S. Minico, S. Galvagno, Catal. Lett. 51 (1998) 41.
[31] P.R. Davies, N.G. Newton, Surf. Sci. 546 (2003) 149.
[32] Z.Z. Lin, T. Okuhara, M. Misono, K. Tohji, Y. Udagawa, J. Chem. Soc. Chem. Commun. (1986) 1673.
[33] S. Takenaka, T. Shimizu, K. Otsuka, Int. J. Hydrogen Energy 29 (2004) 1065.
[34] M. Boudart, M.A. McDonald, J. Phys. Chem. 88 (1984) 2185.
[35] K. Asakura, Y. Iwasara, J. Chem. Soc. Faraday Trans. 86 (1990) 2657.
[36] R.A. Dalla Betta, M. Shelef, J. Catal. 48 (1977) 111.
[37] J.G. Ekerdt, A.T. Bell, J. Catal. 58 (1979) 170.
[38] H. Yamasaki, K. Yoshihiro, Y. Kobori, S. Naito, T. Ohnishi, K. Tamaru, J. Chem. Soc. Faraday Trans. 77 (1980) 2913.
[39] R.D. Kelley, D.W. Goodman, in: D.A. King, D.P. Woodruff (Eds.), Fundamental Studies of Heterogeneous Catalysis, vol. 4, Elsevier Scientific Publishing, Amsterdam, 1982 (Chapter 10).
[40] N.M. Gupta, V.S. Kamble, V.B. Kartha, R.M. Iyer, K.R. Thampi, M. Gratzel, J. Catal. 146 (1994) 173.
[41] N.M. Gupta, A.K. Tripathi, Bull. Catal. Soc. India (2003) 213.
[42] A.L. Kustov, A.M. Frey, K.E. Larsen, T. Johannessen, J.K. Nørskov, C.H. Christensen, Appl. Catal. A 320 (2007) 98.
[43] M.P. Andersson, F. Abild-Pedersen, I.N. Remediakis, T. Bligaard, G. Jones, J. Engbμk, O. Lytken, S. Horch, J.H. Nielsen, J. Sehested, J.R. Rostrup-Nielsen, J.K. Nørskov, I. Chorkendorff, J. Catal. 255 (2008) 6.
[44] O.R. Inderwildi, S.J. Jenkins, D.A. King, J. Phys. Chem. C 112 (2008) 1305.
[45] O. Inderwildi, P. Jenkins, Chem. Soc. Rev. 37 (2008) 2274.
[46] O. Inderwildi, J.S. Jenkins, D. King, Angew. Chem. 47 (2008) 5253.
[47] H. Schubert, U. Guntow, K. Hofmann, R. Schlögl, Fresenius J. Anal. Chem. 356 (1996) 127.
[48] P.B. Weisz, Chem. Eng. Progr. Symp. Ser. 55 (1992) 29.
[49] M.M. Schubert, M.J. Kahlich, H.A. Gasteiger, R.J. Behm, J. Power Sources 84 (1999) 175.
[50] I.M. Hamadeh, P.R. Griffiths, Appl. Spectrosc. 41 (1987) 682.
[51] F. Meunier, D. Reid, A. Goguet, S. Shekhtman, C. Hardacre, R. Burch, W. Deng, M. Flytzani-Stephanopoulos, J. Catal. 247 (2007) 269.
[52] I.-G. Bajusz, J.G. Goodwin Jr., J. Catal. 169 (1997) 157.
[53] V.P. Londhe, V.S. Kamble, N.M. Gupta, J. Mol. Catal. A 121 (1997) 33.
[54] S.J. Fujita, T. Notbutsune, Chem. Eng. J. 68 (1997) 63.
[55] V.P. Londhe, N.M. Gupta, J. Catal. 169 (1997) 415.
[56] R.L. Gorring, A.J. de Rosset, J. Catal. 3 (1964) 341.
[57] H. Knözinger, Y. Zhao, B. Tesche, R. Barth, R. Epstein, B.C. Gates, J.P. Scott, Faraday Discuss. 72 (1981) 53.
[58] J. Zhang, M. Li, Z. Feng, J. Chen, C. Li, J. Phys. Chem. B 110 (2006) 927.
[59] E. Guglielminotti, A. Zecchina, A. Bossi, M. Camia, J. Catal. 74 (1982) 240.
[60] R.D. Gonzalez, M.F. Brown, J. Phys. Chem. 80 (1976) 1731.
[61] A.A. Davydov, A.T. Bell, J. Catal. 49 (1977) 332.
[62] F. Solymosi, J. Raskó, J. Catal. 15 (1989) 107.
[63] G.H. Yokomizo, C. Louis, A.T. Bell, J. Catal. 120 (1989) 1.
[64] E. Guglielminotti, G.C. Bond, J. Chem. Soc. Faraday Trans. 86 (1990) 979.
[65] N.M. Gupta, V.S. Kamble, R.M. Iyer, T. Ravindranathan, M. Grätzel, J. Catal. 137 (1992) 473.
[66] M.W. McQuire, C.H. Rochester, J. Catal. 141 (1993) 355.
[67] S.Z.H. Todorova, G.B. Kadinov, Res. Chem. Intermed. 28 (2002) 291.
[68] H. Pfnür, D. Menzel, F.M. Hoffmann, A. Ortega, A.M. Bradshaw, Surf. Sci. 93 (1980) 431.
[69] J. Assmann, E. Loffler, A. Birkner, M. Muhler, Catal. Today 85 (2003) 235.
[70] H. Knözinger, P. Ratnasamy, Catal. Rev. 17 (1978) 31.
[71] S.T. Yong, K. Hidajat, S. Kawi, J. Power Sources 131 (2004) 91.
[72] C.S. Kellner, A.T. Bell, J. Catal. 71 (1981) 296.
[73] F. Solymosi, A. Erdöhelyi, M. Kocsis, J. Catal. 65 (1980) 428.
[74] V. Sanchez-Escribando, M.A. Larrubia Vargas, E. Finocchio, G. Busca, Appl. Catal. A 316 (2007) 68.
[75] T. Yamada, K.-I. Tanaka, J. Am. Chem. Soc. 113 (1991) 1173.
[76] C.K. Rofer-DePoorter, Chem. Rev. 81 (1981) 447.
[77] M.M. Marwood, R. Doepper, A. Renken, Appl. Catal. A 151 (1997) 223.
[78] R. Leppelt, B. Schumacher, V. Plzak, M. Kinne, R.J. Behm, J. Catal. 244 (2006) 137.
[79] A.S. Wexler, Spectrochim. Acta 21 (1965) 1725.